ABSTRACT

Title: SIMULATION OF DYNAMIC PRESSURE-SWING GAS SORPTION IN POLYMERS

Heather Jane St. Pierre, Master of Science, 2005

Directed By: Professor Timothy A. Barbari
Department of Chemical Engineering

A transport model was developed to simulate a dynamic pressure-swing sorption process that separates binary gas mixtures using a packed bed of non-porous spherical polymer particles. The model was solved numerically using eigenfunction expansion, and its accuracy verified by the analytical solution for mass uptake from a finite volume. Results show the process has a strong dependence on gas solubility. The magnitudes and differences in gas diffusivities have the greatest effect on determining an optimal particle radius, time to attain steady-state operation, and overall cycle time. Sorption and transport parameters for three different polyimides and one copolyimide were used to determine the degree of separation for CO_2/CH_4 and O_2/N_2 binary gas mixtures. The separation results for this process compare favorably to those for membrane separation using the same polymer, and significantly improved performance when a second stage is added to the pressure-swing process.

SIMULATION OF DYNAMIC PRESSURE-SWING GAS SORPTION IN POLYMERS

by

Heather Jane St. Pierre

Thesis submitted to the Faculty of the Graduate School of the
University of Maryland, College Park, in partial fulfillment
of the requirements for the degree of
Master of Science
2005

Advisory Committee:
Professor Timothy A. Barbari, Chair
Associate Professor Raymond A. Adomaitis
Associate Professor Peter Kofinas

Acknowledgements

I would like to thank my advisor, Professor Barbari, for all of his help and guidance during the course of this research. In the short time I have worked for him, I have learned much from the sharing of his knowledge and experience. I would also like to thank my 'co-advisor,' Professor Adomaitis for the use of his Matlab code for the simulations presented in this work. Even though I was not officially a student of his, he always had time to help, and I have learned much from working with him as well.

Table of Contents

List of Tables

List of Figures

Chapter 1: Background

Gas separation processes have evolved over the years to continually improve component separation, as well as increase cost effectiveness and efficiency. Many of these techniques have included variations of membrane separation, pressure-swing adsorption (PSA), liquid absorption, and cryogenic separation. These processes are often economically compared based on the rate of production of separated components and quality of separation.[1]

Two separations of particular commercial interest include carbon dioxide/methane separation and air (oxygen/nitrogen) separation. Current CO_2/CH_4 separation applications include biogas separation from landfills or farms for energy use, natural gas sweetening where CO_2 is removed from natural gas wells, or enhanced oil recovery where supercritical or near critical CO_2 is pumped into oil wells to reduce oil viscosity for easier extraction.[2,3] Air separation applications currently in use include oxygen enrichment for combustion or medical needs, inert gas blanketing on some oil tankers, or nitrogen blanketing for shipping or storing food.[2] These separations have been achieved by using polymeric membrane materials in addition to the more traditional methods.[2] The economic choice of separation process for both CO_2/CH_4 and O_2/N_2 is highly dependent on the scale of that process. In general, membranes have been favored at smaller scales.[1]

Separation using polymer membranes has become an effective means of achieving gas separation in recent years. Typical polymers used in commercial

membrane separation have been polysulfones, polycarbonates and cellulose acetates.[3,4] Recently, focus has turned to polyimides due to their excellent properties for separation. Some of these polyimides have been formed into hollow-fiber membranes,[5,6] but few are commercially available because of their cost and difficulty to manufacture.[2,4]

The formation of integrally-asymmetric hollow fibers in itself is not a simple task. Separation is not determined by the polymer properties alone, but on how the fibers themselves are prepared to provide a defect-free thin film with the proper orientation to maximize separation.[3,6,7] Creating a polymer solution with the desired thermodynamic and rheological properties to form hollow fibers is another challenge associated with this process.[3] Once the fibers themselves are constructed, there is also the issue of bundling them together to be used as a separation device for either bore or shell feed, depending on the application.[2] Lastly, an appropriate fiber length must be chosen to prohibit significant pressure drop in the bore of the hollow fibers.[2]

Given this difficulty in production, an alternative method for separation is proposed here that utilizes the separation characteristics of highly selective polymers by forming them into dense particles and using them in a packed bed. These particles could potentially be formed by spray drying a polymer solution, or in situations where a solution cannot be formed, by simply grinding the polymer into smaller particles. The use of sorbent polymer particles was developed and modeled by Barbari et al.[8] for liquid-liquid extraction in a well-mixed batch process. In this work, the focus instead will be on gas separation.

In this thesis, the separation of binary gas pairs, CO_2/CH_4 and O_2/N_2, is modeled using a dynamic pressure-swing sorption process with dense polymer particles. Two

different polyimides are used for each gas pair, and their separation performance compared to a simple membrane process which utilizes the separation properties of the same polyimide. Although this process does not utilize a steady-state flux, separation results from this model will be shown to be comparable to a membrane separation process.

Chapter 2: Model Formulation

2.1 Process Description

As an alternative to membrane separation, the gas separation process described here uses dynamic pressure-swing sorption. This single-stage process utilizes a separation bed consisting of a vessel packed with nonporous polymer spheres of uniform radius; the schematic can be seen in Figure 2.1. The concept for this process is based on the liquid batch extraction process developed by Barbari et al.[8] For the development of this specific model, two gases will be separated based on their differing solubility and diffusivity in the polymer phase. To take advantage of the different diffusivities, the process is stopped prior to equilibrium, given that at equilibrium, only solubility differences dominate separation. The proposed separation process cycle is composed of three basic steps:

1) The packed bed is charged with a compressed gas mixture to a set pressure with valves 2 and 3 closed. When the desired pressure is reached, valve 1 is closed.
2) The gas in the external phase is sorbed by the polymer particles. At the end of the sorption step, the remaining external phase is purged by opening valve 2 and lowering the pressure to P_2 (taken to be 0 atm for the simulations of this work). After the remaining gas in the external phase has been expelled, valve 2 is closed.

3) Valve 3 is opened, and vacuum is applied to allow the mass in the particles to desorb. After a given time, valve 3 is closed, and the separation bed is re-charged with the compressed gas mixture (step 1).

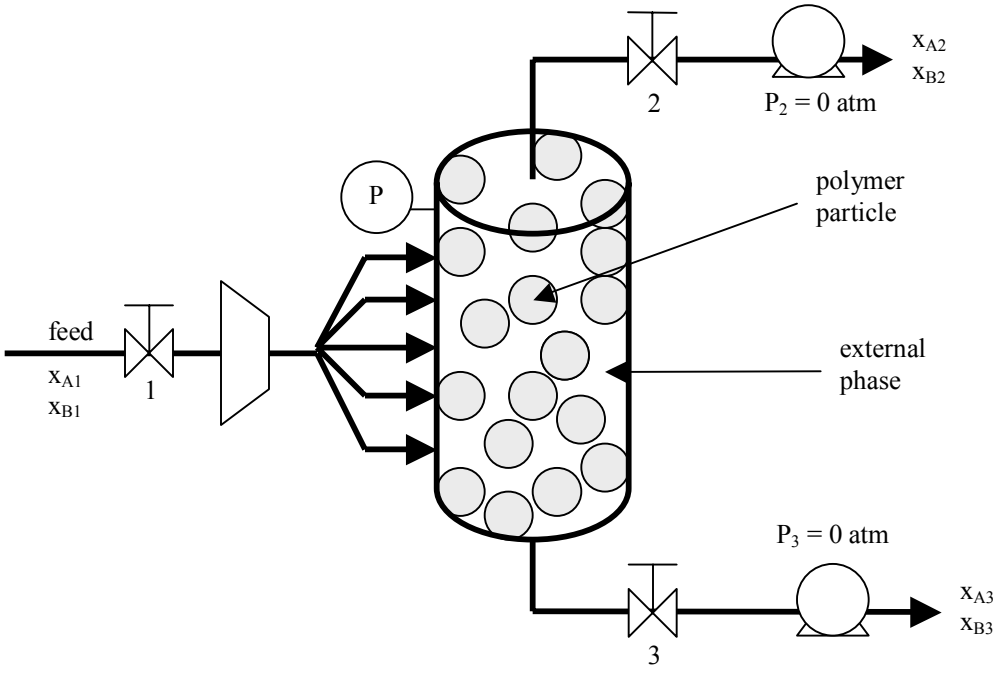

Figure 2.1. Schematic of the gas separation apparatus using polymer particles of a uniform radius. A manifold is used on the feed to ensure a rapid fill time.

A few assumptions and process simplifications were made to ensure an accurate estimation of the physical results. First, a manifold is used to ensure a short fill time relative to the sorption time scale, so an initial external phase concentration could be determined. For the purposes of the model, the sorption time scale was between 22 and 130 seconds for the specified polymers, making this a valid assumption. In addition, the process is assumed to be isothermal. Ideal gas behavior was also assumed, allowing no change in gas compressibility with pressure. The specific parameters used for the simulations in this thesis are listed in Table 2.1.

Separation bed volume	1L
Polymer phase volume fraction (constant)	0.5
Particle radius (uniform, constant)	50-100μm
Temperature (isothermal)	35°C
Feed pressure	20 atm
Desorption pressure	0 atm

Table 2.1. List of parameters used in this work to model the dynamic pressure-swing sorption separation process.

2.2 Continuity Equation and Boundary Conditions

The continuity equation that accounts for the mass transport of each species into and out of the polymer phase is as follows:

$$\frac{\partial C_i}{\partial t} = D_i \frac{1}{r^2} \frac{\partial}{\partial r}\left(r^2 \frac{\partial C_i}{\partial r} \right) \tag{2.1}$$

where r is the radial position in the spherical polymer particle, C_i is the concentration of component 'i' and D_i is the diffusion coefficient of species 'i' in the polymer. These equations assume that the diffusion coefficient for each species is independent of concentration. It is also assumed that the diffusion coefficient for mass transport into the particles is the same for mass transport out.

At the start of the initial cycle, the polymer particles are assumed to be free of any gas, therefore:

$$\text{at } t = 0, \text{ for all } r: \qquad C_i = 0$$

In addition, there is no flux at the plane of symmetry, or center of the spherical particles:

$$\text{at } r = 0, \text{ for all } t: \qquad \frac{\partial C_i}{\partial r} = 0$$

The final boundary condition allows for a mass balance between the external and polymer phases, as this specific process involves mass uptake from a finite external volume. This boundary condition is at the interface between the polymer and external phase, where the rate the gas leaves the external phase is equal to the rate the gas enters the polymer phase at the boundary:

$$\text{at } r = R, \text{ for all } t: \qquad \frac{V_e}{S_i}\left[\frac{\partial C_i}{\partial t}\right]_{r=R} = -D_i V_p \frac{3}{R}\left[\frac{\partial C_i}{\partial r}\right]_{r=R} \tag{2.2}$$

where S_i is the partition (or solubility) coefficient of component 'i' in the polymer phase, and V_e and V_p are the external and polymer phase volumes, respectively. The partition coefficients used here are defined as the ratio of the concentration in the particle relative to the concentration in the external phase, and is assumed to be independent of concentration.

The external (or gas) phase is assumed to be well-mixed at all times; therefore, convective mass transfer resistance at the polymer surface is negligible. This assumption is reasonable because the diffusion coefficient in many polymers (and those used in this study) is on the order of 10^{-7} to 10^{-8} cm^2/s, while that in the gas phase is 10^{-1} cm^2/s. In addition, the gas sorbed into the polymer is assumed to have no swelling effects on the polymer, allowing the external and polymer phase volumes to be assumed constant. Given the operating time scales of the experiment, the densities of the polymers chosen, a polymer volume fraction of 0.5, and an initial pressure of 20 atm, the maximum possible

increase in polymer mass if all of the gas was sorbed by the polymer particles is only 1.6%. These specific parameters will be discussed later in Chapter 3.

2.3 Eigenfunction Expansion Solution Procedure

The process developed here is dynamic, and therefore cannot be represented or estimated by an equilibrium analytical solution. The methods of finite differences and finite element can be used to solve the partial differential equation listed in the previous section, but these methods do not account for the entire volume of the particle, nor can they capture concentration profile behavior at the particle interface. In addition, the stability of the finite differences and finite element solution is based on the size of the time step relative to the spatial step size. Eigenfunction expansion models the concentration profiles over the entire particle radius, and its solution accuracy is only controlled by the truncation number, or number of basis functions, therefore it is the method of choice for this simulation.

The concentration profiles in time and space can be approximated as the summation of an infinite number of functions:

$$C(r,t) = \sum_{i=1}^{\infty} a_i(t)\psi_i(r) + f(t) \tag{2.3}$$

where $a_i(t)$ are coefficients determined from the given initial condition and *f(t)* is the finite-volume, concentration boundary condition that varies with time. The $\psi_i(r)$ in Equation 2.3 are the orthogonal basis functions generated by the non-trivial solutions to the Sturm-Liouville equation over $0 < r < 1$:

$$\frac{1}{r^2}\frac{d}{dr}\left(r^2\frac{d\psi}{dr}\right)=\lambda\psi \qquad \text{or} \qquad \nabla^2\psi_i=\lambda_i\psi_i \tag{2.4}$$

subject to:

$$a\frac{d\psi(0)}{dr}+b\psi(0)=0$$

$$c\frac{d\psi(1)}{dr}+d\psi(1)=0$$

where λ_i are the eigenvalues of the basis functions. These basis functions for the Sturm-Liouville equation were determined using Matlab code written by Adomaitis[9] and solved using Matlab SV Release13.

The time derivative of this estimation for the concentration profiles can then be substituted into the original conservation equation (Equation 2.1) which can be written as:

$$\dot{C} = D\nabla^2 C$$

$$\sum_{i=1}^{\infty}\dot{a}_i\psi_i+\dot{f}=D\sum_{i=1}^{\infty}a_i\nabla^2\psi_i \tag{2.5}$$

Substituting the Sturm-Liouville equation (Equation 2.4) into Equation 2.5 and multiplying both sides of the resultant equation by ψ_j yields:

$$\sum_{i=1}^{\infty}\dot{a}_i\psi_i\psi_j+\dot{f}\psi_j=D\sum_{i=1}^{\infty}a_i\lambda_i\psi_i\psi_j$$

Integrating both sides of this equation over the volume of the spherical particles, and taking into account the orthogonality of the basis functions, a relationship for the coefficients can be determined:

$$\dot{a}_j=Da_j\lambda_j-\dot{f}I_j \tag{2.6}$$

$$\text{where} \quad j = 1,2,3\ldots \quad \text{and} \quad I_j = \int_0^R \psi_j 4\pi r^2 dr$$

Since *f(t)* is the boundary condition at the particle surface, $\dot{f}$ can be determined using the flux boundary condition at the surface, solving Equation 2.2 for the time derivative of the concentration at the boundary:

$$\dot{f} = \dot{C}(R,t) = -S\frac{V_p}{V_e}\frac{3}{R}D\left[\frac{\partial C}{\partial r}\right]_{r=R} \tag{2.7}$$

Substituting the approximation for the concentration profile solution (Equation 2.1) into Equation 2.7 gives:

$$\dot{f} = -K\sum_{i=1}^{\infty} a_i \left[\frac{\partial \psi_i}{\partial r}\right]_{r=R} \tag{2.8}$$

$$\text{where } K = S\frac{V_p}{V_e}\frac{3}{R}D$$

Now that the equations for $\dot{f}$ and a relationship between $\dot{a}$ and a have been established, Equation 2.8 can be substituted into Equation 2.6 and placed into matrix-vector form to be solved by a linear ordinary differential equations solver:

$$\begin{bmatrix} \dot{a}_1 \\ \dot{a}_2 \\ \vdots \\ \dot{a}_j \\ \dot{f} \end{bmatrix} = \begin{bmatrix} D\lambda_1 + I_1 K\left[\frac{\partial \psi_1}{\partial r}\right]_{r=R} & I_1 K\left[\frac{\partial \psi_2}{\partial r}\right]_{r=R} & \cdots & I_1 K\left[\frac{\partial \psi_j}{\partial r}\right]_{r=R} & 0 \\ I_2 K\left[\frac{\partial \psi_1}{\partial r}\right]_{r=R} & D\lambda_2 + I_2 K\left[\frac{\partial \psi_2}{\partial r}\right]_{r=R} & \cdots & I_2 K\left[\frac{\partial \psi_j}{\partial r}\right]_{r=R} & 0 \\ \vdots & \vdots & \vdots & \vdots & \vdots \\ I_j K\left[\frac{\partial \psi_1}{\partial r}\right]_{r=R} & I_j K\left[\frac{\partial \psi_2}{\partial r}\right]_{r=R} & \cdots & D\lambda_j + I_j K\left[\frac{\partial \psi_j}{\partial r}\right]_{r=R} & 0 \\ -K\left[\frac{\partial \psi_1}{\partial r}\right]_{r=R} & -K\left[\frac{\partial \psi_2}{\partial r}\right]_{r=R} & \cdots & -K\left[\frac{\partial \psi_j}{\partial r}\right]_{r=R} & 0 \end{bmatrix} \begin{bmatrix} a_1 \\ a_2 \\ \vdots \\ a_j \\ f \end{bmatrix}$$

This system of ordinary differential equations (ODE) was solved with Matlab using a linear ODE solver written by Adomaitis.[9] Once the coefficients (a_i) and concentration at the boundary (*f*) are determined for each time step, this information is then substituted back into the original equation for the estimation of the concentration profiles (Equation 2.3) used to model the process discussed in this thesis.

Once the concentration profiles are determined, they can be used to find the mass uptake in the polymer particles. The number of moles of *i* in the polymer phase at a given time can be found by integrating the corresponding concentration profile over the volume of a particle, multiplied by the number of particles, N_p:

$$n_i(t) = 4\pi N_p \int_0^R C_i(r,t) r^2 dr \tag{2.9}$$

This calculation is used to determine the majority of the results in this work, including the mass balance of each gas in the polymer and gas phases and the separation performance of the dynamic pressure-swing process described in this chapter.

Chapter 3: Model Verification

Due to the dynamic nature of the sorption/desorption process modeled here, it was important to verify the behavior of the mass transport model presented in the Chapter 2. To affirm the accuracy of the model, the numerical solution was compared to two different known solutions: an analytical solution and the solution to these partial differential equations using the method of finite differences.

3.1 Comparison to Analytical Solution

The numerical solution was compared to the results of the analytical solution for the time-dependent mass uptake of a spherical particle in a well-mixed solution of limited volume found by Crank[10] and given as:

$$\frac{n(t)}{n_\infty} = 1 - \sum_{n=1}^{\infty} \frac{6\beta(\beta+1)\exp(-q_n^2\tau)}{9+9\beta+q_n^2\beta^2} \tag{3.1}$$

where the q_n's are the nontrivial solutions to

$$\tan q_n = \frac{3q_n}{3+\beta q_n^2} \tag{3.2}$$

τ is a dimensionless time variable defined as

$$\tau = \frac{Dt}{R^2} \tag{3.3}$$

and β is the ratio of the external mass of penetrant to the polymer phase penetrant mass, applying the partition coefficient S

$$\beta = \frac{V_e}{SN_p\left(\frac{4}{3}\pi R^3\right)}$$

where N_p is the number of polymer particles in the system. For the purposes of the solution comparison, the external and polymer phase volumes were taken to be equal; therefore, β simplified to $1/S$. The solutions to Equations 3.1 and 3.2 were computed using Matlab and compared to the numerical solution, as shown in Figure 3.1. For this comparison, values of $S = 5$, $D = 2\times10^{-8}$ cm^2/s, and $R = 1\times10^{-3}$ cm were used for both

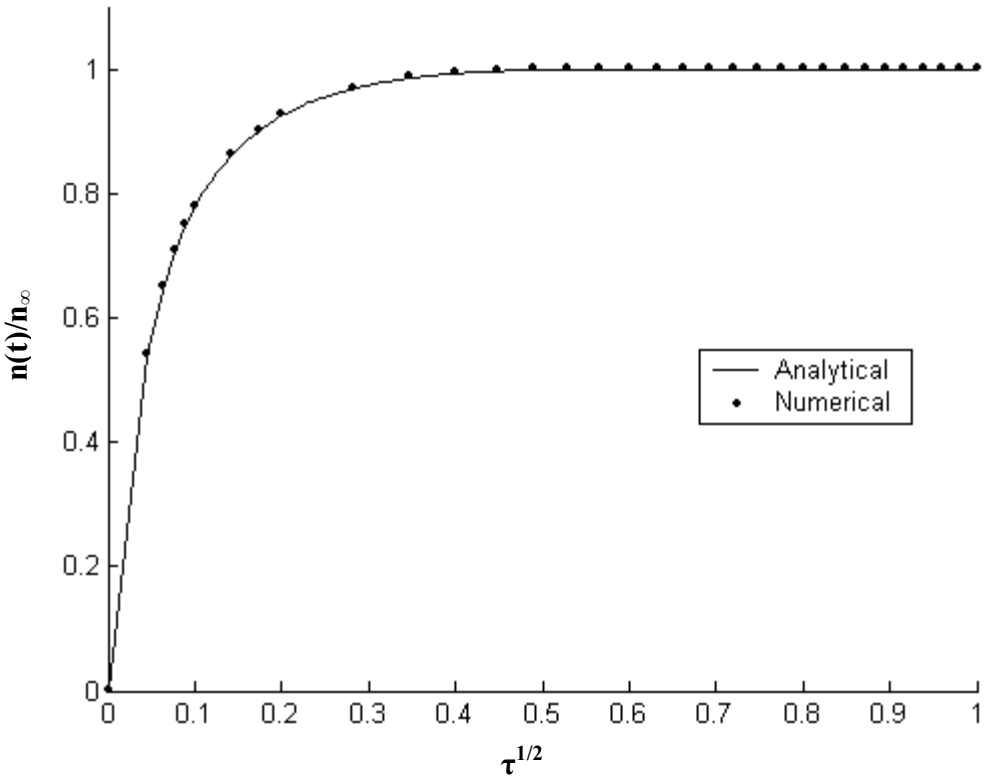

Figure 3.1. Plot of polymer mass uptake against the dimensionless time variable, $\tau^{1/2}$, comparing the numerical solution to the analytical solution developed by Crank[10] shown in Equation 3.1.

the analytical and numerical solutions. To obtain the best estimate for the exact solution, the first 5000 terms of the summation were used. 250 basis functions were used to compute the eigenfunction expansion solution. Figure 3.1 verifies the accuracy of the numerical solution when compared to the exact solution, where the largest root mean squared error observed between the two solutions using 250 basis functions was 4.0×10^{-3} (0.5% error) at $\tau^{1/2} = 0.1$.

3.2 Comparison to Method of Finite Differences

To further verify the accuracy of the numerical solution, the eigenfunction expansion solution was also compared to the solution obtained by Barbari et al.[8] who used the method of finite differences. To determine an optimal time and polymeric particle radius for their liquid-liquid batch separation process, Barbari et al.[8] plotted component selectivity against the square root of the dimensionless time variable, τ, where selectivity was defined as:

$$\alpha_{A/B} = \frac{(n_A / n_B)}{(C_{Ae} / C_{Be})} \tag{3.4}$$

where n_i is the number of moles of component i in the polymer phase and C_{ie} is the concentration of component i in the external phase. The results are compared graphically, in Figure 3.2. Values of $S_A = 5$ and $S_B = 1$ were used for both calculation methods. 250 basis functions were used to find the eigenfunction expansion solution. The close comparison of these plots (Figure 3.2), in combination with the excellent comparison to the exact solution (Figure 3.1), verifies the accuracy of the eigenfunction expansion solution.

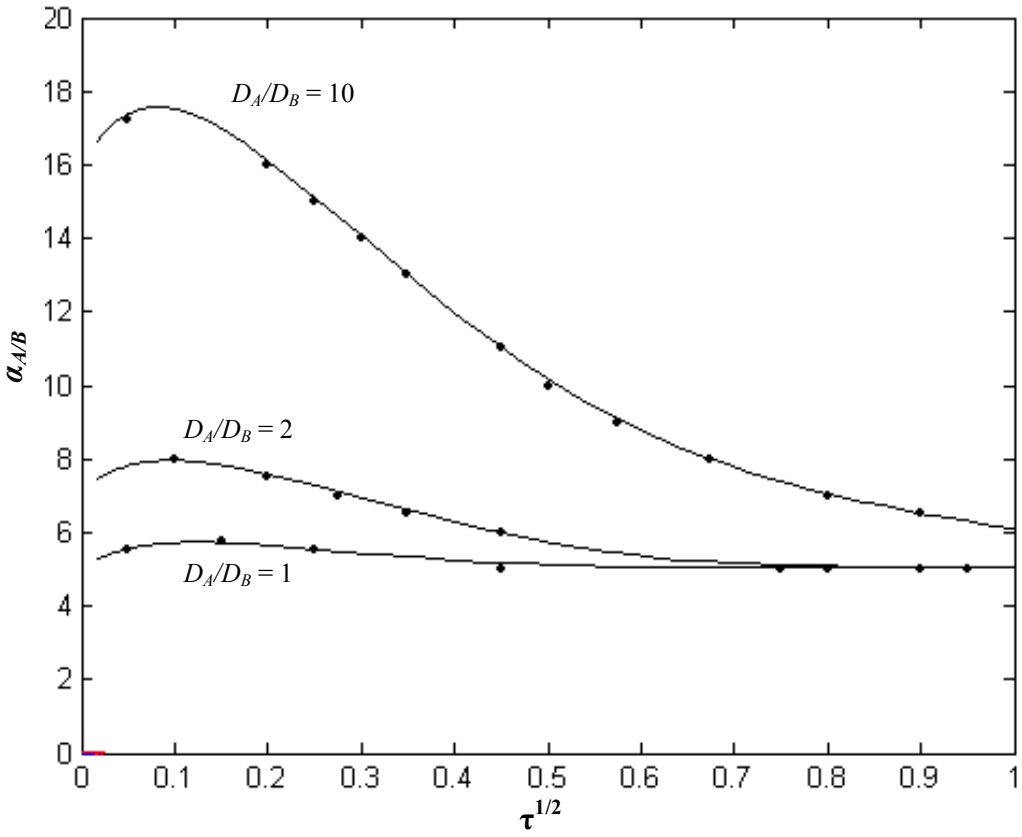

Figure 3.2. Plot of selectivity, $\alpha_{A/B}$, (Equation 3.4) vs. $\tau^{1/2}$ (Equation 3.3) using eigenfunction expansion and finite differences. The solid lines are the results from the eigenfunction expansion solution, and the points are the results found by Barbari et al.[8] using the method of finite differences.

3.3 Comparison to Equilibrium Calculations

The final test for accuracy compared the calculations from the model at equilibrium conditions to known values of concentration or mass uptake at equilibrium. To best understand these comparisons, it is important to introduce the ideal selectivity between components A and B ($\alpha^*_{A/B}$), which is defined as:

$$\alpha^*_{A/B} = \frac{S_A D_A}{S_B D_B} \tag{3.4}$$

where S_i is the solubility (or partition) coefficient and D_i is the diffusivity of component *i*. For a membrane, $\alpha^*_{A/B}$ is equal to the membrane permeability ratio, P_A/P_B, where the permeability for component *i* is:

$$P_i = S_i D_i \tag{3.5}$$

For this dynamic process, $\alpha^*_{A/B}$ physically represents the ratio of initial fluxes at the interface $r = R$.

When looking at selectivity, for short time scales both the difference in diffusion coefficients (D_A/D_B) and difference in solubilities (S_A/S_B) play a significant role. For long time scales, the diffusion coefficients no longer dominate, and selectivity approaches an equilibrium value of S_A/S_B. This behavior was observed by Barbari et al.,[8] and is also seen in these model results, shown in Figure 3.2. In Figure 3.2, the selectivity approaches the solubility ratio $S_A/S_B = 5$ for all diffusivity ratios at long time scales.

To calculate the exact mass uptake in the polymer particles at infinite time, a basic algebraic relation was developed for a finite volume, where the initial mass of component *i* is equal to the sum of the masses in the polymer and external phases *at equilibrium*:

$$C^\circ_{ie} V_e = C_{ie} V_e + C_{ip} V_p \tag{3.6}$$

where C°_{ie} represents the initial concentration in the external phase, and C_{ip} represents the concentration in the polymer phase. The solubility coefficient is defined as the ratio of polymer phase to external phase concentration:

$$S_i \equiv \frac{C_{ip}}{C_{ie}} \tag{3.7}$$

Substituting this relation into equation (3.6) gives the concentration in the polymer phase at equilibrium, and can be defined in terms of C_{ie}^{o}:

$$C_{ip} = \frac{S_i C_{ie}^{\circ} V_e}{V_e + S_i V_p} \tag{3.8}$$

Since the equilibrium mass uptake of component *i* can be determined by:

$$n_{i\infty} = C_{ip} N_p \frac{4}{3} \pi R^3 \tag{3.9}$$

where N_p is the number of spherical polymer particles, the mass uptake of a component at equilibrium can then be found by:

$$n_{i\infty} = \frac{S_i C_{ie}^{\circ} V_e}{V_e + S_i V_p} N_p \frac{4}{3} \pi R^3 \tag{3.10}$$

Equation 3.10 was used to determine the exact value of the equilibrium mass uptake for each component for the sorption step of the process. To simulate equilibrium conditions, the model time scale was chosen to be 10^4 seconds. For runs using two sets of parameters for each of the two gases, the infinite mass uptake values matched those of the exact solution for the sorption step to four decimal places.

The desorption step solution was verified by assuming an infinite reservoir (open volume, simulated as $V_e / V_p = 10^{30} cm^3$) with an external pressure of 0 atm. The time scale used to simulate equilibrium conditions was 10^4 seconds. The expected behavior at infinite time for an infinite external phase would result in the evacuation of all mass in the polymer particles. For two different sets of parameters for each of the two gases, the final mass in the particles was on the order of 10^{-21} mol, verifying the accuracy of the behavior of the desorption step.

Chapter 4: Model Results and Discussion

4.1 Determination of Optimal Separation Parameters

Once the accuracy of the model was verified, the next step was to determine which parameters will provide the best indication for gas separation potential, specifically for carbon dioxide/methane separation and oxygen/nitrogen separation. Since this pressure-swing separation process deals with many of the same concepts as membrane separation, similar parameters were taken into consideration.

When selecting a polymer for a membrane, the main criteria are membrane stability, mechanical properties, cost, and most importantly, component selectivity (Equation 3.4). For a membrane in steady-state operation with a constant flux, the best inherent separation is obtained by maximizing $\alpha^*_{A/B}$. Like membranes, component solubility and diffusivity are also key factors for the pressure-swing sorption process discussed in this work, but the optimal relationship is not as straightforward.

Since the goal is to maximize the separation of the two gases, it is important to find a polymeric material that has different intermolecular and physical interactions (such as size selectivity) with each of the gases. A high solubility and a high diffusion coefficient in a given polymer result in higher mass uptake of a component at a given period of time compared to one with low solubility and low diffusivity. The ideal polymer for separation would sorb only one gas and leave the other in the external phase, but this is not always possible for gases with small molecular volumes such as CO_2, CH_4, N_2 and O_2.

Since this pressure-swing process does not utilize a steady-state flux as does a membrane process, ideal selectivity is not the sole factor to consider when maximizing separation. In Equation 3.4, selectivity can also be represented as a ratio of mole fractions for each phase (or for a membrane, permeate and retentate), which does not take into account the relative amounts of mass in those phases. For example, in the model presented here, a very small amount of total mass in the polymer could have a high mass ratio (n_A/n_B) due to component A having a very high diffusivity and solubility, but a large amount of mass could still remain in the external phase with a mass ratio near unity. This combination would still result in a high selectivity based on the mass fractions, but would not result in good separation for this process because the amount of mass in the polymer phase relative to the mass in the external phase is ignored. Therefore, the better indicator to determine the optimal length of the sorption cycle is the external phase concentration ratio (C_B/C_A). Maximizing this ratio provides the highest extent of separation in the first outlet stream, where, during the sorption step, the external phase is purged at the time of maximum separation.

The optimal length of the desorption step is much more difficult to determine due to the fact that the separation bed is open to vacuum and effectively, an infinite external phase volume. The main reason for applying vacuum is to minimize mass build-up in the polymer particles prior to subsequent sorption steps. In determining a desorption time, it is important to consider both mass build-up as well as total cycle time. A long desorption step will allow more mass to leave the particle, but could result in an inefficient separation process overall due to an excessively long cycle time, resulting in low product output. Therefore, desorption step times were chosen based on the attainment of a

constant mass retention after successive cycles and the minimization of the number of cycles before this 'steady-state' was reached.

While it is desirable to have one component with high solubility and diffusion coefficients as well as a high solubility ratio, this separation process is not optimized when the ratio of diffusion coefficients is large. This behavior is more pronounced when the sorption and desorption times are equal. The reason for this is that a large difference in diffusion coefficients lends itself to excessive mass buildup of the more slowly diffusing species. After successive sorption and desorption cycles, this accumulation is amplified. Simulation runs with a moderate difference in the diffusivities of the two species will still result in separation, but will not cause mass buildup of the slower species.

The magnitudes of the ideal selectivity and diffusion coefficients also play a role in polymer selection. Solubility and diffusivity ratios were held constant for comparative runs, but their magnitudes were altered to determine their individual contributions to separation by this process. For all parameter combinations, particle radius was held constant and the desorption time was twice that of the sorption time to inhibit mass build up in the polymer phase. The sorption time scale was determined by maximizing the external phase concentration ratio for each set of polymer parameters.

The first comparison considered the magnitude of the diffusivities while the diffusivity ratio remained the same ($D_A/D_B = 2$). To isolate diffusion effects, the solubilities of both components were set equal to 1. The results showed nearly equivalent separation for both the sorption and desorption steps of the separation process, even after the magnitudes of the diffusion coefficients were increased by a factor of 5.

Based on these calculations, it appears that the magnitudes of the diffusion coefficients themselves do not play a major role in separation for this process. However, the absolute value of the diffusivity does determine the optimal sorption/desorption time scale and the polymer particle radius, both of which are important practical factors to be considered for the application of this process.

The second comparison was to determine the effect of the magnitudes of the solubility coefficients, while keeping the solubility ratio constant ($S_A/S_B = 5$). For these tests, the diffusion coefficients were set equal to one another, and the sorption time scale was determined by maximizing the external concentration ratio. The results of this comparison showed the process has a strong dependence on the magnitude of the solubility coefficients. For a 50/50 mixture, increasing the magnitude of the solubilities by a factor of 5 increased separation in the sorption step by 12%, but reduced the separation in the desorption step by 12%. Lower solubilities lead to greater separation in the polymer particle, and therefore greater separation in the desorption step when most of the gas is removed from the polymer phase. The low solubilities also resulted in a 468s (7.8 min) increase in the overall cycle time when the particle radius was held constant.

Lastly, a comparison of the magnitudes of the product of S_i and D_i were made to determine its effect on the separation ability of the process. For the purposes of this test, $(S_AD_A)/(S_BD_B) = 10$. When the product, S_AD_A, was increased by a factor of 25 (increase in diffusivity by a factor of 5 and solubility by a factor of 5), the separation at the end of the sorption step was increased by 14% and the separation at the end of the desorption step was reduced by 10%. Although an increase in the diffusion coefficient alone shows little relative change in separation, the magnitude of the diffusion coefficient appears to

play a minor role in separation for this process when coupled with solubility. The 25-fold increase in magnitude of the S_AD_A product also shortened the sorption time scale by a factor of 10.7.

Based on these results, the magnitudes of S_A and S_AD_A have the greatest effect on achieving the best separation for this pressure-swing sorption process. High S_AD_A and S_A result in greater separation in the sorption step, while low S_AD_A and S_A result in greater separation in the desorption step. Depending on the specific application, good separation can be achieved with low or high values of solubility and the product of solubility and diffusivity. The relative sizes of these values will affect whether or not better separation is attained in the stream rich in the more soluble and faster-diffusing component (desorption step) or in the stream rich in the slower-diffusing, less soluble species (sorption step). The magnitudes of these values will also have a large effect on determining polymer particle radius and sorption/desorption time scale length.

4.2 Polymer Selection

As previously mentioned, important factors to consider when choosing a polymer for a separation process are the solubility, solubility ratio, diffusivity, and diffusivity ratio. There is a considerable amount of literature on the separation of CO_2/CH_4 and O_2/N_2 using many different polymers as membrane materials, with polyimides providing excellent separation properties for both sets of gases discussed here.

Polyimides show excellent mechanical strength as well temperature and chemical resistance.[3] Aromatic polyimides, such as 6FDA-ODA, 6FDA-DAF, 6FDA-*p*-DDS, and copolyimide 6FDA-durene/mPDA (80/20) have rigid backbones, and their overall

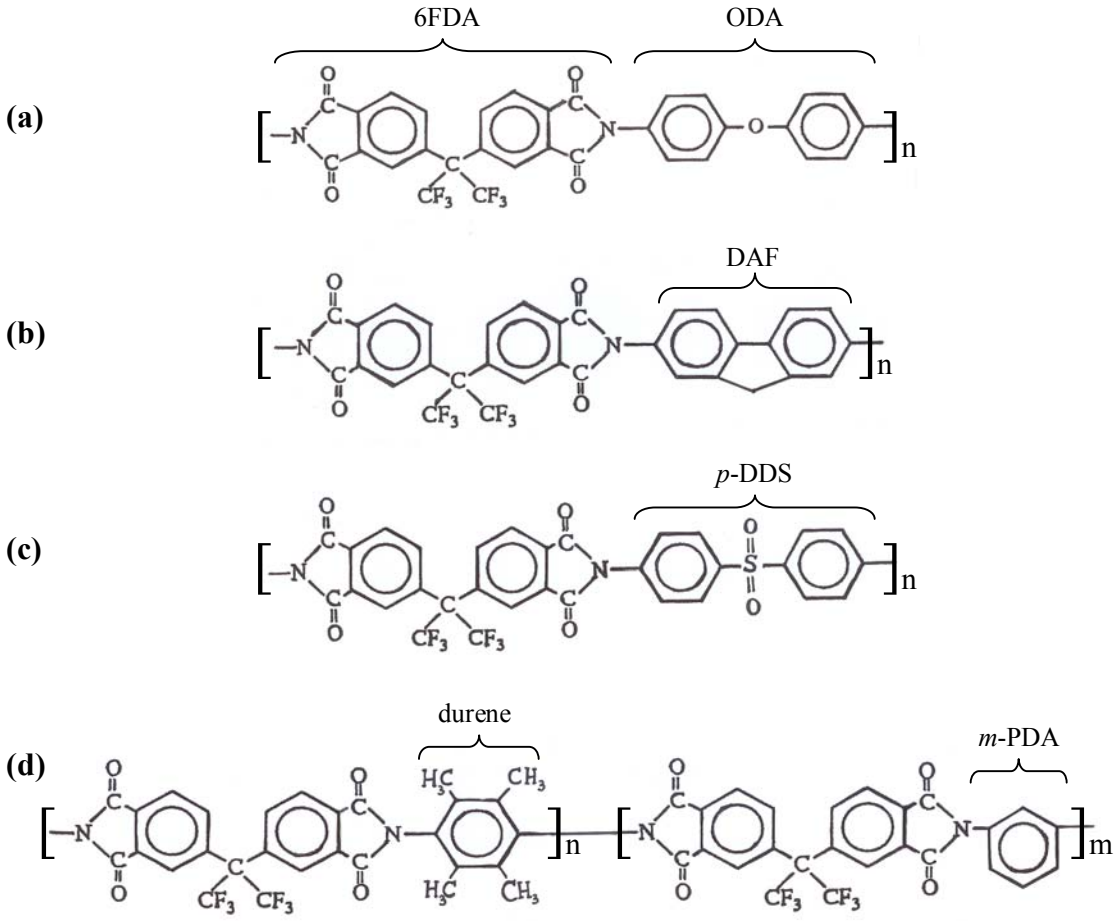

Figure 4.1. Chemical structures of the repeat units of the polyimides (a) 6FDA-ODA, (b) 6FDA-DAF, (c) 6FDA-*p*-DDS, and (d) 6FDA-durene/mPDA copolymer.

structures can be seen in Figure 4.1. As a result of this rigidity, a 'frozen' free volume is formed due to regular voids.[3] In addition, there is a structural hindrance to packing in the 6FDA polyimides[3,4,11] due to the bulky CF_3 groups, adding to the free volume in the polymer. Free volume is important in increasing diffusivity, but an important balance must be reached between diffusivity and diffusivity selectivity (D_A/D_B). Packing density also plays a role in size selectivity, so ideally a polymer would have enough free volume to allow high diffusivities, but a low enough packing density that the material can still be selective. Polyimides have greater diffusivity selectivity compared to traditional

Polymer	D_{CO2}	D_{CO2}/D_{CH4}	S_{CO2}	S_{CO2}/S_{CH4}
6FDA-ODA[12]	3.58	16.3	5.52	3.70
6FDA-p-DDS[4]	2.1	12.0	6.26	3.80
Polymer	**D_{O2}**	**D_{O2}/D_{N2}**	**S_{O2}**	**S_{O2}/S_{N2}**
6FDA-DAF[12]	4.92	3.47	1.35	1.78
6FDA-durene/ mPDA (80/20)[13]	32.47	3.71	1.59	1.08

Table 4.1. Diffusion coefficients and solubilities of gases in selected polymers at 35ºC and 10 atm (O_2 data is at 2 atm). Diffusion coefficients are in units of 10^{-8} cm^2/s. Solubility coefficients are in dimensionless form, calculated with an assumed compressibility of 1. Superscripts refer to the reference numbers.

membrane materials, such as polysulfone and polycarbonate, because they possess a higher packing density.[4] These data can be seen in Table 4.1. Ideal membrane permeability for each of these polymers can be found for a given gas by Equation 3.5. These values will be used for the pressure-swing sorption simulation and membrane calculations to be discussed later in the chapter.

As stated earlier, component solubility is another important separation parameter for this process. Since solubility is mainly influenced by intermolecular interactions, aromatic polyimides are of interest because they have many functional groups available for these interactions. The polyimides shown in Figure 4.1 have electron-rich areas, available to donate electrons, and areas of electron acceptors; these characteristics allow for greater separation[4] between CO_2/CH_4 and O_2/N_2. Absent any intermolecular interactions, the solubility coefficient was shown to increase with increasing free volume.[3]

Due to the fact that CO_2 and CH_4 have very small differences in kinetic diameter[14] (3.3Å and 3.8Å, respectively) the difference in solubility between the two components is mainly due to the interactions with the polymer. Since CO_2 is a quadrupole, it has strong quadrupole-dipole interactions with the polar carbonyl and CF_3 groups in the 6FDA polyimides. In comparison, CH_4 is a non-polar molecule, and engages in weaker van der Waals interactions with the non-polar groups in the polymer, resulting in a lower relative solubility.

Although helpful in enhancing differences in solubility, these molecular interactions between polyimides and CO_2 can potentially have negative effects on the process, such as polymer swelling. This swelling has been shown by Wind et al.[15] to affect the long-term diffusivity and selectivity of similar polyimides. The plasticizer effect of CO_2 has been shown to cause an increase in CO_2 diffusivity over time.[15] It is not the purpose of this work to model this time-dependent effect, but it is an important factor to consider in future applications for CO_2 separation.

Due to their similar respective kinetic diameters[14] of 3.46 and 3.64, O_2 and N_2 have typically been very difficult to separate using polymers. A small difference in critical temperature and condensability between the two molecules results in differing solubilities in polyimides;[3, 13] this difference shows the potential for the use of polyimides as air separation membranes.

Based on the separation parameters discussed earlier, it is important to weigh optimal separation with practical factors such as particle radius, process time scale, and time to reach 'steady-state.' High diffusivities will result in better separation in the sorption step and will lead to a shorter time scale length; therefore, the magnitudes of

these coefficients are important. Also as important is the ratio of diffusivities. A high diffusion coefficient ratio results in greater separation, but if the ratio is too high, the desorption time scale must be significantly lengthened to inhibit excessive mass retention of the more slowly diffusing species in the polymer particles. As a result, a high diffusivity ratio will also result in a longer time to reach 'steady-state' for the entire sorption/desorption process, as it will take more cycles for the mass retention to reach a pseudo-equilibrium. The optimal separation parameters are high diffusivities, a moderate diffusivity ratio, high solubilities, and a high solubility ratio.

4.3 Specifications for Carbon Dioxide/Methane Separation

As discussed previously, CO_2 and CH_4 have different molecular characteristics which allow for their separation. Two examples of polyimides that best capitalize on these differences are 6FDA-ODA and 6FDA-*p*-DDS, whose structures can be seen in Figure 4.1. The ODA has a higher diffusion coefficient ratio, a lower solubility coefficient ratio, higher diffusivities, and lower solubilities relative to *p*-DDS (Table 4.1).

4.3.1 Comparison to Polymer Characteristics for CO_2/CH_4 Separation

Polymer comparisons were conducted on the basis of several process factors, including sorption separation, desorption separation, and overall cycle time based on the attainment of an equilibrium mass retention inside the polymer particles. Many of the separation processes for CO_2/CH_4 mentioned in Chapter 1 utilize feed compositions near a 50/50 mixture;[3] therefore, the model calculations completed here use the same molar

feed ratio. For all calculations involving 6FDA-ODA and 6FDA-*p*-DDS, the desorption time was set equal to three times the sorption time to ensure there was no significant change in mass retention in the particles over long time scales. The sorption time for each polymer was chosen to be the time at which maximum separation occurred in the external phase, based on the external concentration ratio. For long sorption times, the external concentration ratio curve is not as steep, allowing more choices for the optimal separation time scale. This can be seen in Figure 4.2 for CO_2/CH_4 separation. Lastly, the particle radius for both polymers was fixed at 50μm.

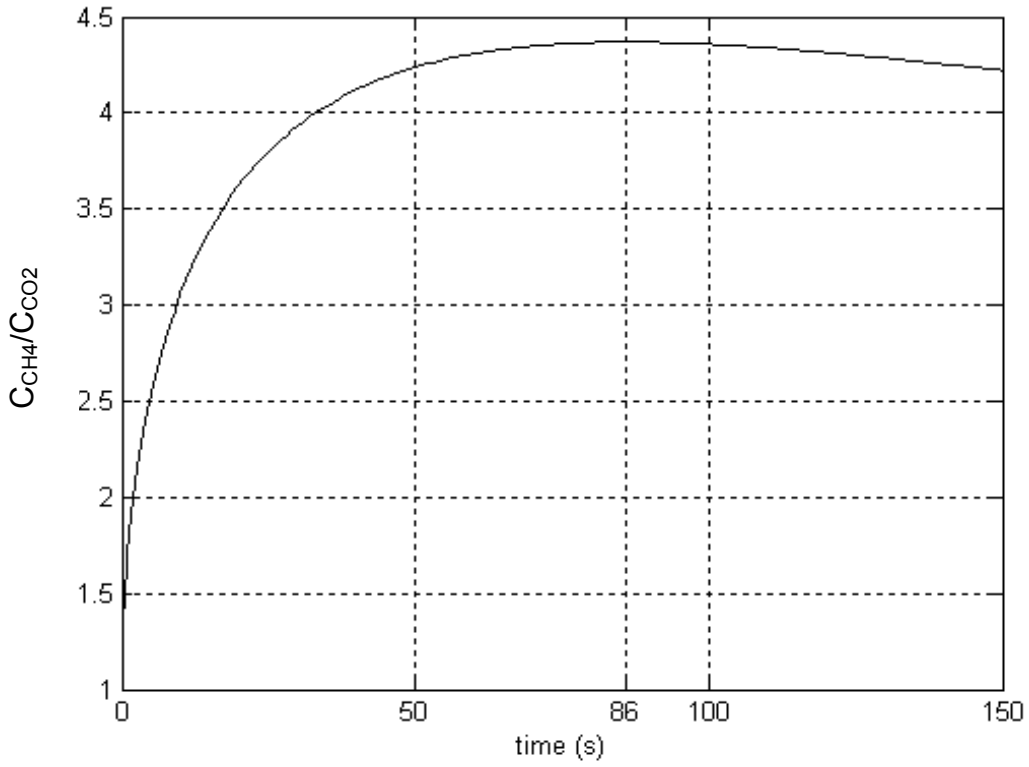

Figure 4.2. Plot of external concentration ratio vs. time for CO_2/CH_4 separation using 6FDA-ODA particles with a radius of 50μm in the dynamic pressure-swing sorption process for a 50/50 feed mixture. The sorption time was determined to be at the time at which the external concentration ratio was at a maximum. In the case of 6FDA-ODA, the maximum ratio occurred at 86s.

Another important issue to take into consideration is the attainment of 'steady-state' conditions for the process, because the separation characteristics are dependent on the amount of mass retained in the polymer particles. This has the greatest effect on the desorption composition, seen in Figure 4.3, where there is a 3% difference in separation from the first to the last cycle. In order to determine the time to reach a constant mass uptake for a given polymer, calculations for 20 successive cycles were run. An important visual reference is the shape of the concentration profiles in the polymer particles at the end of the desorption step. If the final profile of a given component has a significant maximum anywhere other than at the center of the particle, the mass build-up of the given component has not reached pseudo-equilibrium, and the particle will continue to retain additional mass. Once the final profile exhibits an overall constant or decreasing trend from the center of the particle to the interface, 'steady-state' has been reached and additional mass will not migrate towards the center of the particle and accumulate after successive runs. This behavior can be seen in comparing Figures 4.4-4.7 for the separation of CO_2 and CH_4 using 6FDA-ODA.

Based on the model results for a 50/50 mixture, the 6FDA-*p*-DDS showed only a 1% improvement in separation for the sorption step and a 3% improvement in the desorption step (Table 4.2). Both polymers showed nearly the same CH_4 mass retention at the end of the desorption step, but 'steady-state' mass uptake occurred in the *p*-DDS derivative after 12 cycles, whereas 'steady-state' occurred in the ODA derivative in 14 cycles. Plots of the mass uptake for successive cycles can be seen in Figure 4.8. Lastly, the sorption step times were calculated to be 130s for the *p*-DDS derivative and 86s for

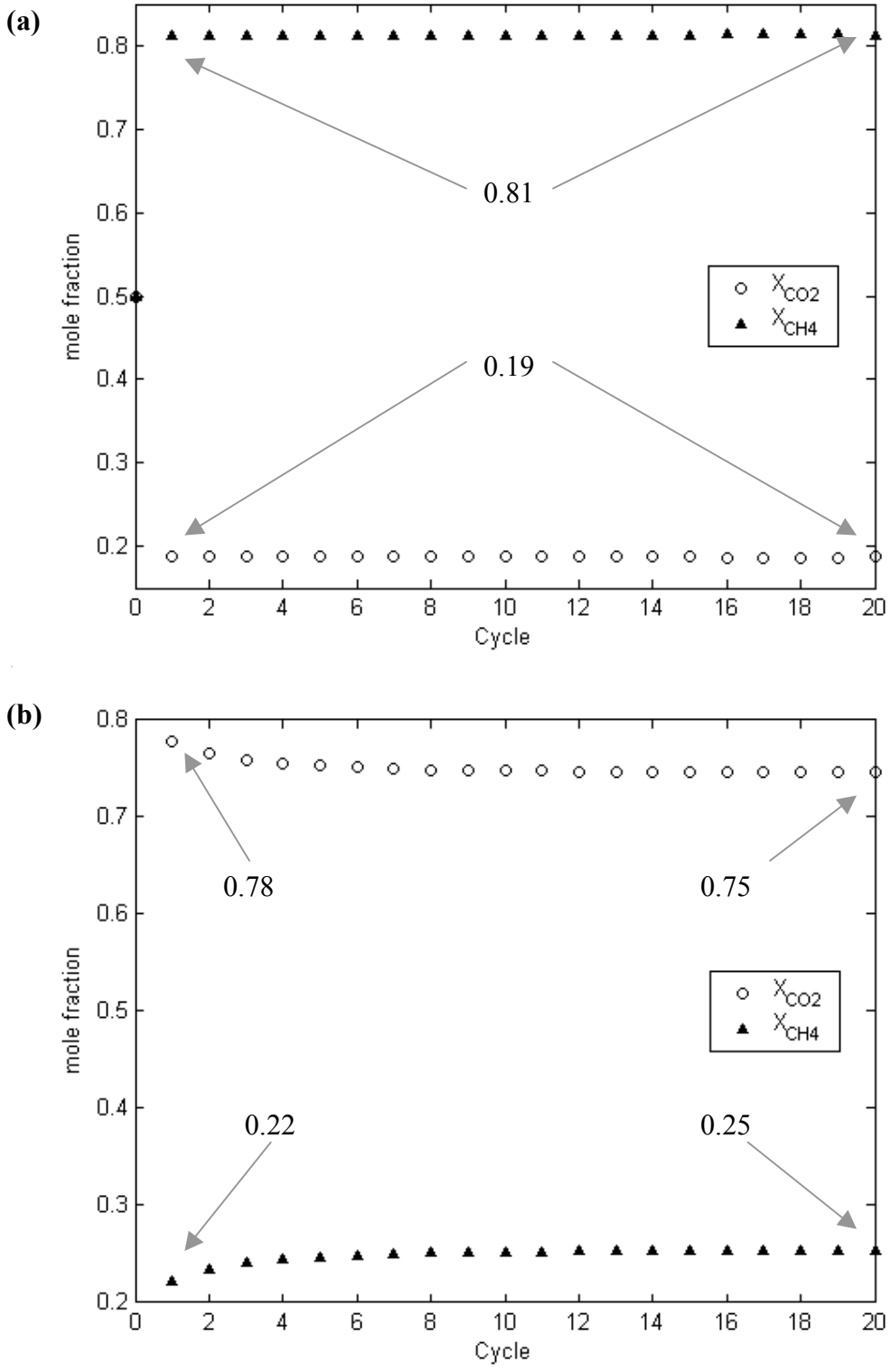

Figure 4.3. Plots of mole fraction at the end of the (a) sorption and (b) desorption steps for successive cycles using 6FDA-ODA for separation of a 50/50 mixture of CO_2/CH_4 using the dynamic pressure-swing sorption process.

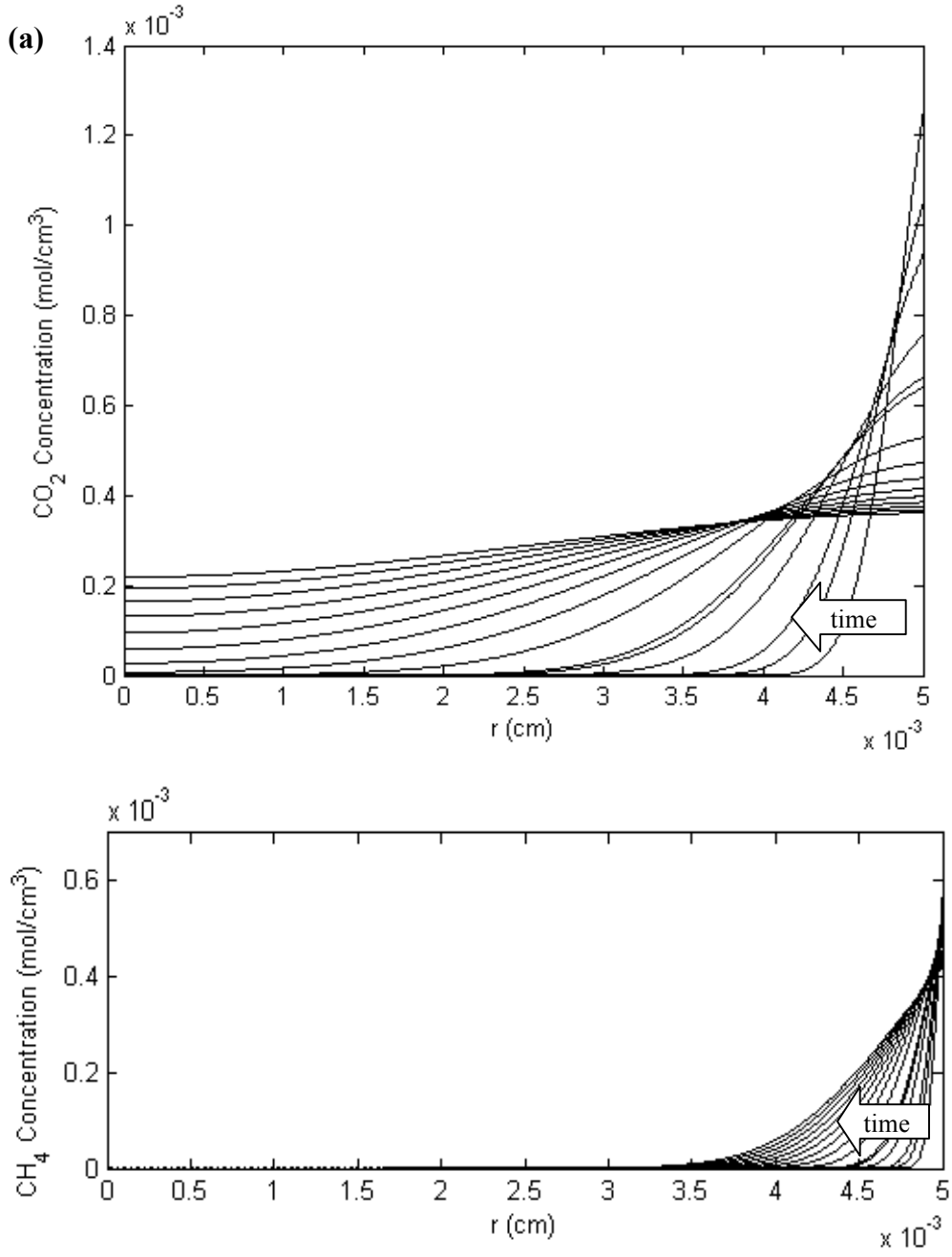

Figure 4.4. Plots of the concentration profiles for the *initial sorption step* in the spherical polymer particles over time for pressure-swing sorption separation of a 50/50 mixture of CO_2/CH_4 using 6FDA-ODA. (a) CO_2 concentration profiles. (b) CH_4 concentration profiles. The time steps for both plots were t = 1 2 3 6 9 10 18 26 34 42 50 58 66 74 82s.

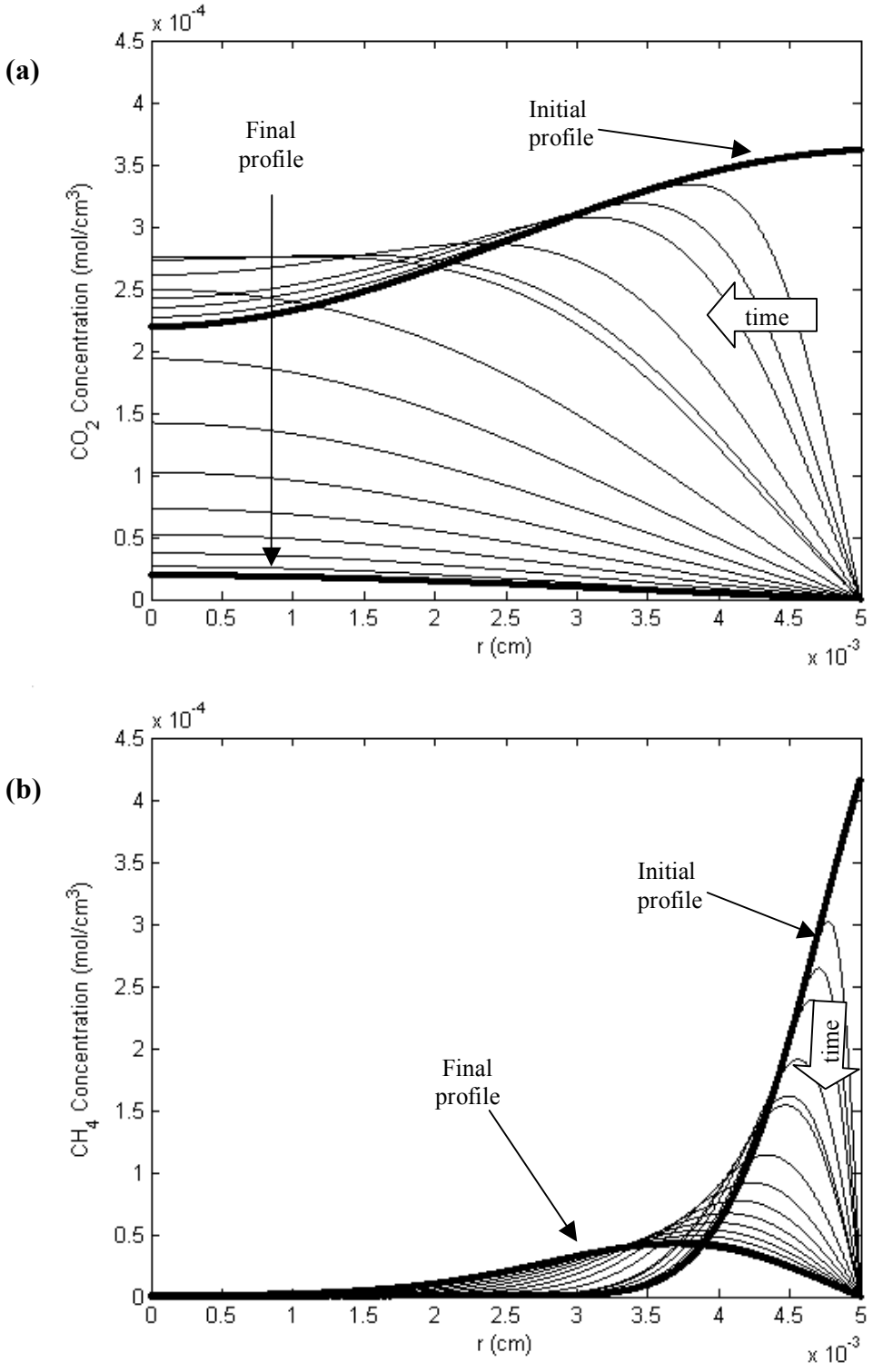

Figure 4.5. Plots of concentration profiles for the *initial desorption step* in the polymer particles over time for pressure-swing sorption separation of a 50/50 CO_2/CH_4 gas mixture. (a) CO_2 concentration profiles. (b) CH_4 concentration profiles. The initial and final concentration profiles are highlighted. The time steps for each plot were t = 3 6 9 18 27 30 54 78 102 126 150 174 198 222 246s.

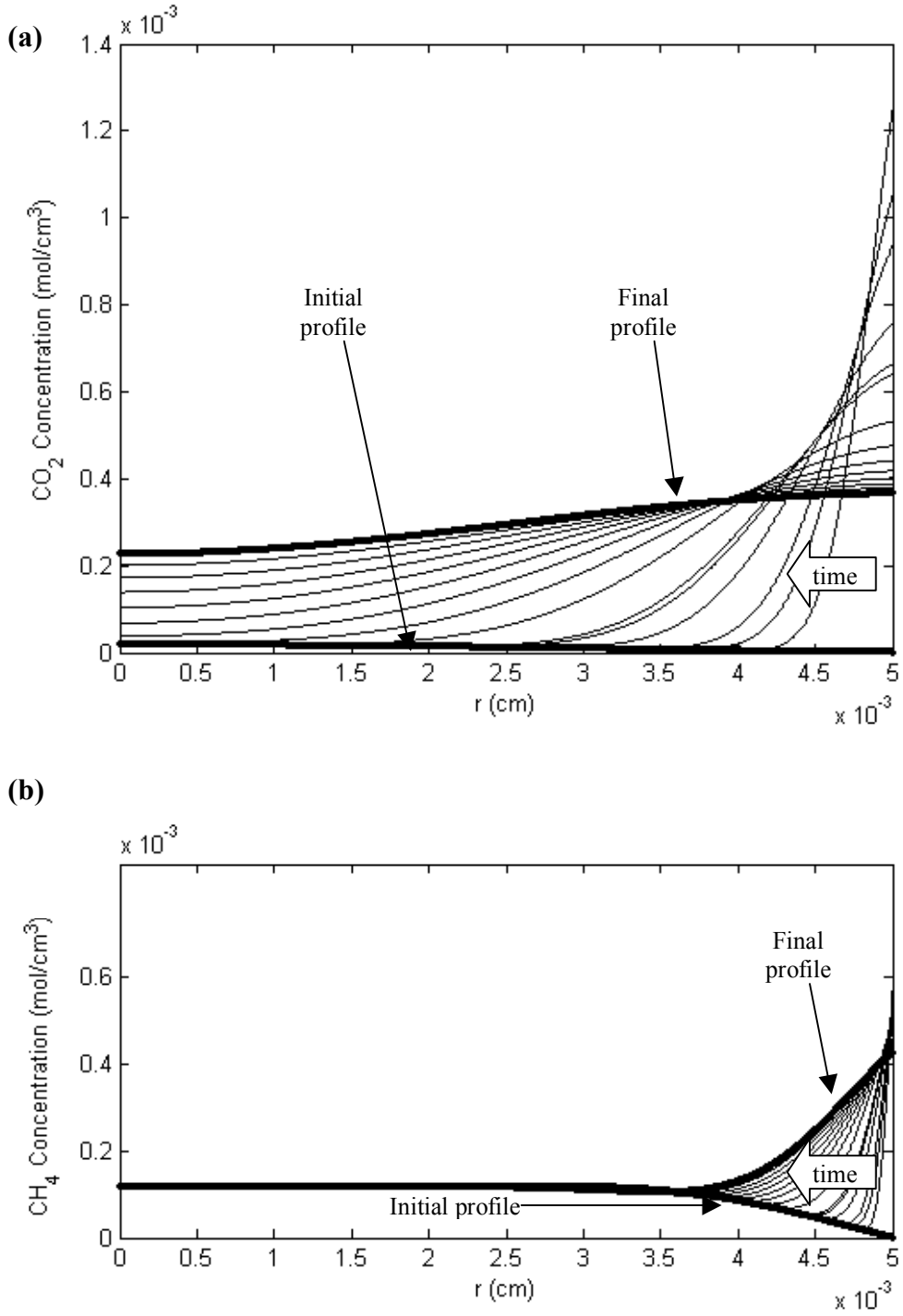

Figure 4.6. Plots of *'steady-state' sorption* concentration profiles in the polymer particles over time for pressure-swing sorption separation of a 50/50 CO_2/CH_4 gas mixture. (a) CO_2 concentration profiles. (b) CH_4 concentration profiles. The initial and final concentration profiles are highlighted. The time steps for each plot were t = 1 2 3 6 9 10 18 26 34 42 50 58 66 74 82s.

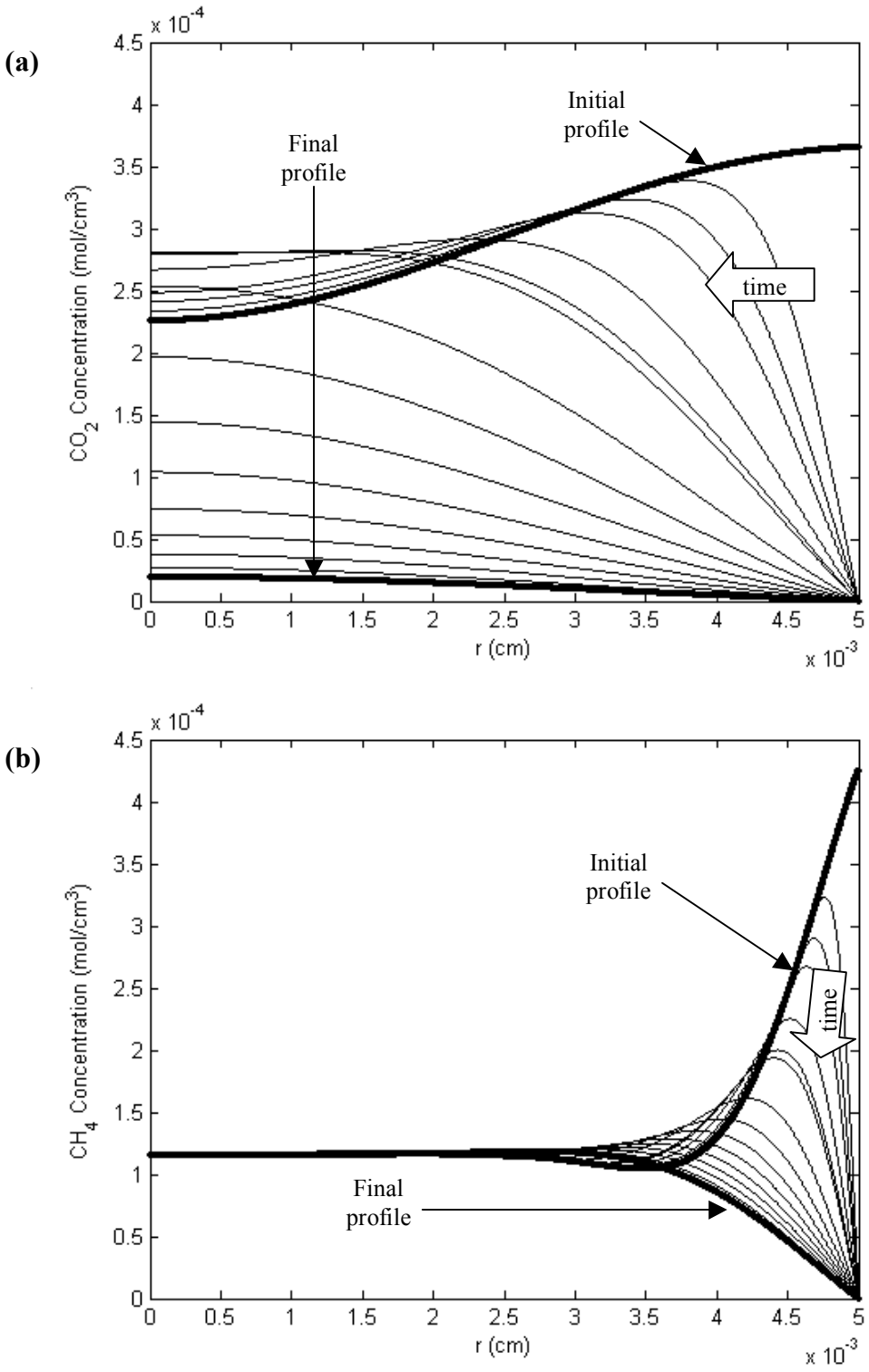

Figure 4.7. Plots of *'steady-state' desorption* concentration profiles in the polymer particles over time for pressure-swing sorption separation of a 50/50 CO_2/CH_4 gas mixture. (a) CO_2 concentration profiles. (b) CH_4 concentration profiles. The initial and final concentration profiles are highlighted. The time steps for each plot were t = 3 6 9 18 27 30 54 78 102 126 150 174 198 222 246s.

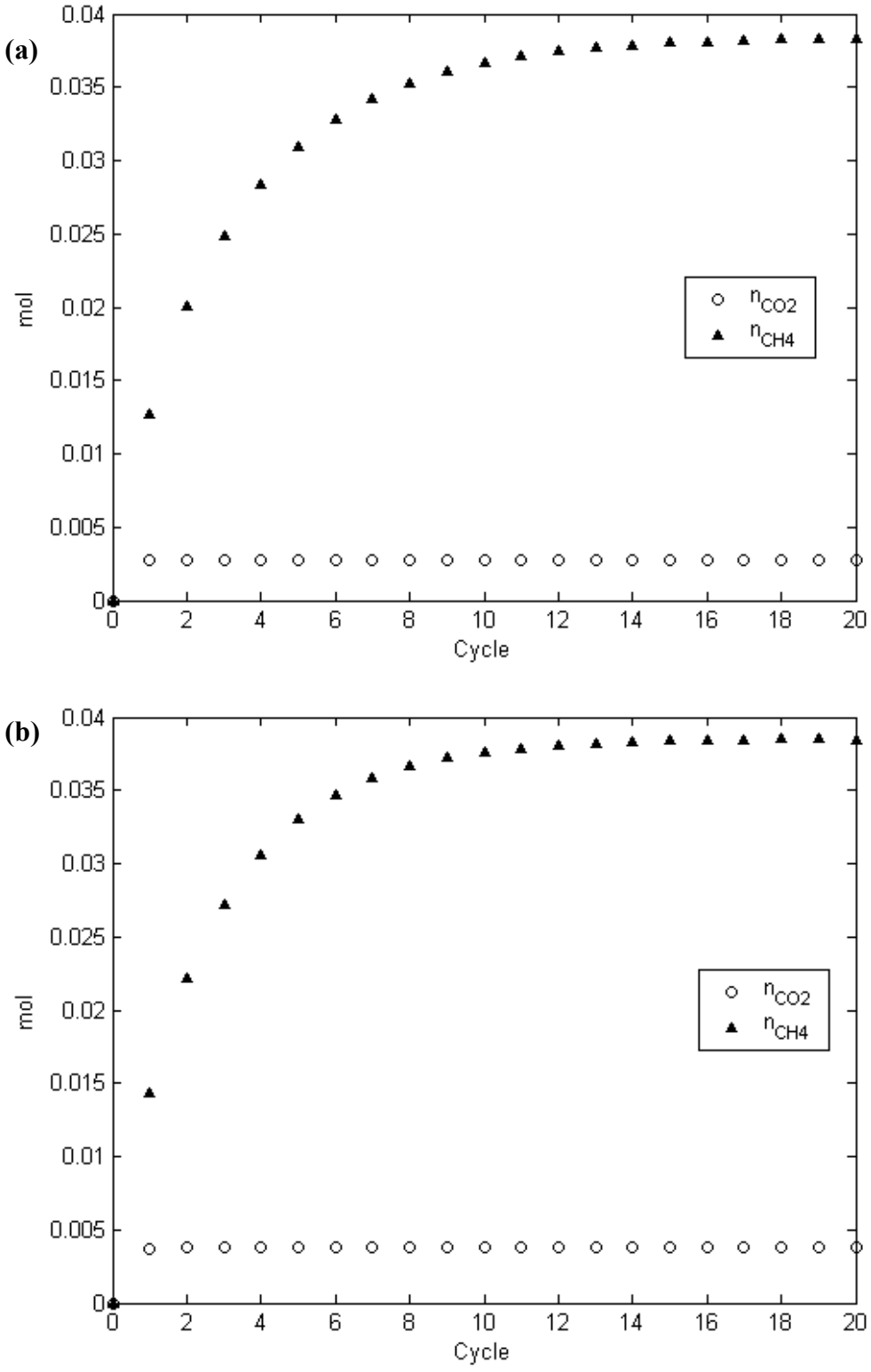

Figure 4.8. Plot of moles of CO_2 and CH_4 remaining in the polymer particles after successive separation cycles based on a 50/50 feed mixture at 20 atm, 1L total volume, equal volumes of polymer and external phases. (a) 6FDA-ODA. (b) 6FDA-*p*-DDS.

Polymer	Sorption Step (Gas Phase)		Desorption Step (Gas Phase)	
	X_{CO2}/X_{CH4}	Step Time (s)	X_{CO2}/X_{CH4}	Step Time (s)
6FDA-ODA	0.19 / 0.81	86	0.75 / 0.25	258
6FDA-*p*-DDS	0.18 / 0.82	130	0.72 / 0.28	390

Table 4.2. Comparison of polymer performance in separating a 50/50 mixture of CO2 and CH4 using pressure swing sorption at an initial pressure of 20 atm

the ODA derivative (Table 4.2). This step time difference results in a 66% reduction in overall cycle time for ODA relative to *p*-DDS.

Given the small difference in separation gained by the p-DDS group compared to the ODA group, the better of the two polymers for this process is 6FDA-ODA given the significantly smaller cycle time length. This reduction in cycle time increases flow rate and production, which allows for more efficient operation of this process.

4.3.2 Comparison to Membrane Technology for CO_2/CH_4 Separation

In order to determine the relative effectiveness of the pressure-swing process, some simple calculations were made to determine the separation ability of a membrane composed of the same polymer for comparison. The membrane calculation used is based on material balance equations, transport equations, and ideal selectivity, and was taken from *Separation Process Principles*.[16]

The membrane calculation requires permeabilities as defined by Equation 4.1, as well as a stage cut, defined as:

$$\theta = \frac{n_p}{n_f} \tag{4.2}$$

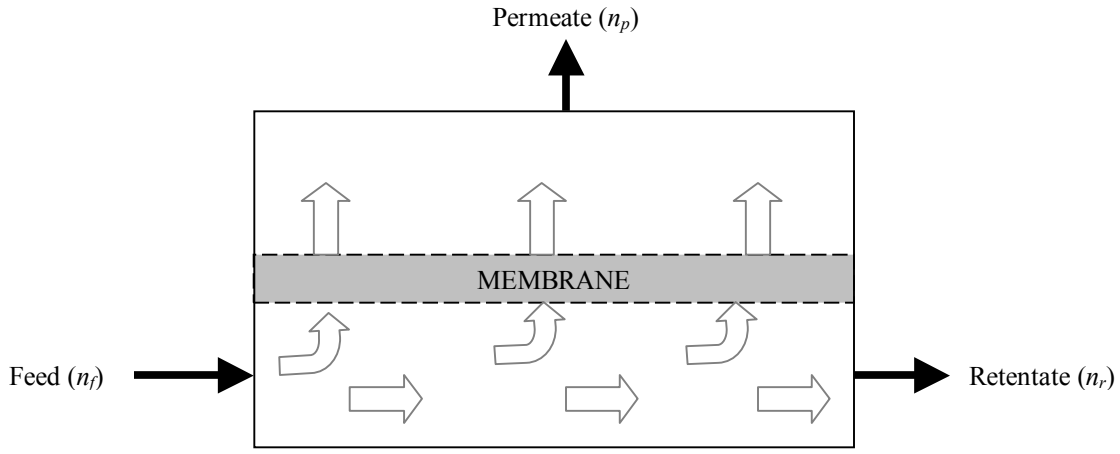

Figure 4.9. Schematic of a simple steady-state membrane separation process.

where n_p is the molar flow rate of the permeate and n_f is the molar flow rate of the feed. These definitions are explained in Figure 4.9. The stage cut used for the membrane comparison for both polysulfone (PSF) and 6FDA-ODA was the same as that for the feed and moles removed after the desorption step for CO_2/CH_4 separation using 6FDA-ODA. The feed flow rate and permeate flow rate were taken as the number of moles of feed and moles removed from the polymer at the end of the desorption step, respectively, divided by the total cycle time.

All nonlinear equations were solved using Polymath 5.1. Since most commercial membranes have an active layer thickness[17] of 1000-2000Å, a thickness of 1000Å was used for these calculations. For the purposes of the membrane comparison calculation, the feed pressure was assumed to be held constant at 20 atm, and the permeate pressure was assumed to be 0 atm. The membrane permeabilities for 6FDA-ODA were found using the data in Table 4.1 and Equation 3.5. The permeability[11] for CO_2 in PSF is

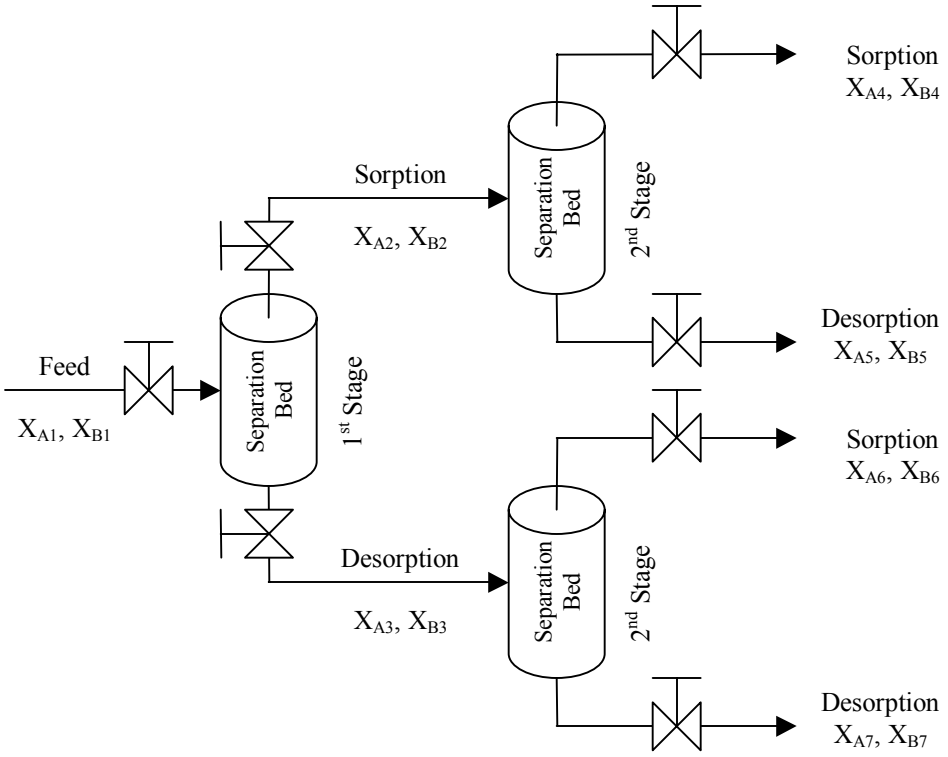

Figure 4.10. Simple schematic for the dynamic pressure-swing sorption process with a 2nd stage added.

4.8×10^{-8} cm^3 (STP) cm^{-1} atm^{-1} s^{-1} and the permeability ratio[11] for CO_2/CH_4 separation is 21.9.

A second stage was added to the pressure-swing sorption process to compare to membrane performance. The second stage was calculated by passing the separated gas from the first sorption and desorption steps through another set of separation beds. This concept is shown in Figure 4.10. For the purposes of the second stage calculation, the mole fractions of the sorption and desorption steps of the second stage were used at a pressure of 20 atm.

Comparing the membrane retentate to the sorption step and the permeate to the desorption step purge in this process, a membrane composed of 6FDA-ODA gives a

retentate that is nearly the same as the gas in the external phase, and a permeate that is 17% higher in CO_2 that the external phase after a desorption. If a second stage is applied to the CH_4-rich stream, a very high separation (95% CH_4) is achieved in the sorption step from the second separation bed. The CO_2-rich stream can also be separated further by a second separation bed, resulting in a stream very close in composition to the membrane permeate. These values are compared in Table 4.3, where all dynamic pressure-swing sorption values given are those calculated for the process after 20 successive cycles. The 40/60 mixtures from the desorption step from the second stage of the CH_4-rich stream (x_{A5}/x_{B5} in Figure 4.10) and from the sorption step of the second stage of the

Process	Sorption Step (Gas Phase)	Desorption Step (Gas Phase)	
	X_{CO2} / X_{CH4}	Stage Cut (θ)	X_{CO2} / X_{CH4}
Pressure-Swing Sorption: (6FDA-ODA)			
1st Stage	**0.19 / 0.81**	0.56	**0.75 / 0.25**
2nd Stage w/ 1st Stage Sorption Product	**0.05 / 0.95**	0.39	0.40 / 0.60
2nd Stage w/ 1st Stage Desorption Product	0.40 / 0.60	0.70	**0.90 / 0.10**
Membrane:			
6FDA-ODA	**0.17 / 0.83** (retentate)	0.56	**0.92 / 0.08** (permeate)
PSF	**0.14 / 0.86** (retentate)	0.56	**0.78 / 0.22** (permeate)

Table 4.3. Results of separating a 50/50 mixture of CO_2 and CH_4 using the pressure-swing sorption process for 6FDA-ODA at an initial pressure of 20 atm. The 2nd stage calculations used the mole fractions from the sorption step and desorption step purges at a pressure of 20 atm. These results are compared to a membrane process.[16] 6FDA-ODA and PSF properties were used for the membrane calculations.

CO_2-rich stream (x_{A6}/x_{B6} in Figure 4.10) suggest the potential to recycle these back to the feed for greater process efficiency. With only one second stage applied to the CO_2-rich stream from the first stage, the pressure-swing sorption is comparable to a membrane separation with the same polymer (Table 4.3).

Since PSF is used to make a commercial CO_2/CH_4 membrane,[2] a calculation using its properties was also completed to compare to the pressure-swing process. The single-stage process compares very well in terms of separation performance and is within 5% of the retentate composition and within 3% of the permeate composition. A second stage for the two gas streams extracted after the sorption and desorption steps shows significant improvement over the PSF membrane, as shown in Table 4.3.

4.4 Specifications for Oxygen/Nitrogen Separation

Since O_2 and N_2 have very similar characteristics, they have historically been very difficult to separate. However, polyimides have shown promise in providing greater separation, as compared to typical membrane materials such as polycarbonate and polysulfone.[11] Two such types of polyimides are 6FDA-DAF and the copolyimide (80/20) 6FDA-durene/mPDA (Figure 4.1). The attached durene and mPDA groups provide a higher diffusion coefficient ratio, a lower solubility ratio (near unity), higher diffusivities, and higher solubilities relative to the DAF group (Table 4.1).

4.4.1 Comparison to Polymer Characteristics for O_2/N_2 Separation

The same factors from the CO_2/CH_4 process were considered for the O_2/N_2 separation process: separation in the external phase during the sorption step, overall cycle

time, and the attainment of 'steady-state' mass uptake of the slower diffusing species at the end of desorption. The desorption time scale was set equal to twice the sorption time scale due to the closeness in diffusivities of O_2 and N_2. The profile behavior and verification of the 'steady-state' operation for O_2/N_2 separation using the copolymer 6FDA-durene/mPDA (80/20) can be seen in Figures 4.11-4.14. The sorption time for each polymer was also set to the value where maximum separation occurred in the external phase. Lastly, to adjust for the high diffusivities and to increase the time scale to a reasonable length relative to the fill time, the particle radius was increased to 100μm for the copolymer 6FDA-durene/mPDA; the particle radius remained 50μm for 6FDA-DAF. For air separation (21% O_2 and 79% N_2) the model results show only a 2% increase in separation from the sorption step when using the DAF polyimide compared to the copolymer. This is shown in Table 4.4, where the separation values given for the pressure-swing process are those calculated after 20 successive cycles. The copolymer has nearly three times the mass build-up in the particle compared to 6FDA-DAF, but this mass retention is only 8% of the original N_2 mass. Near 'steady-state' operation conditions for 6FDA-DAF are reached within 5 cycles, whereas the copolymer takes approximately 8 cycles. This comparison can be seen in Figure 4.15. In terms of the length of the entire cycle, the copolymer reaches steady operation after 9.7 min, while 6FDA-DAF reaches steady operation after 16 min. The copolymer's diffusion and selectivity characteristics also allow for a larger particle radius, and a shorter overall time scale (66s vs. 192s), making 6FDA-durene/mPDA (80/20) the polymer of choice for this process (Table 4.4).

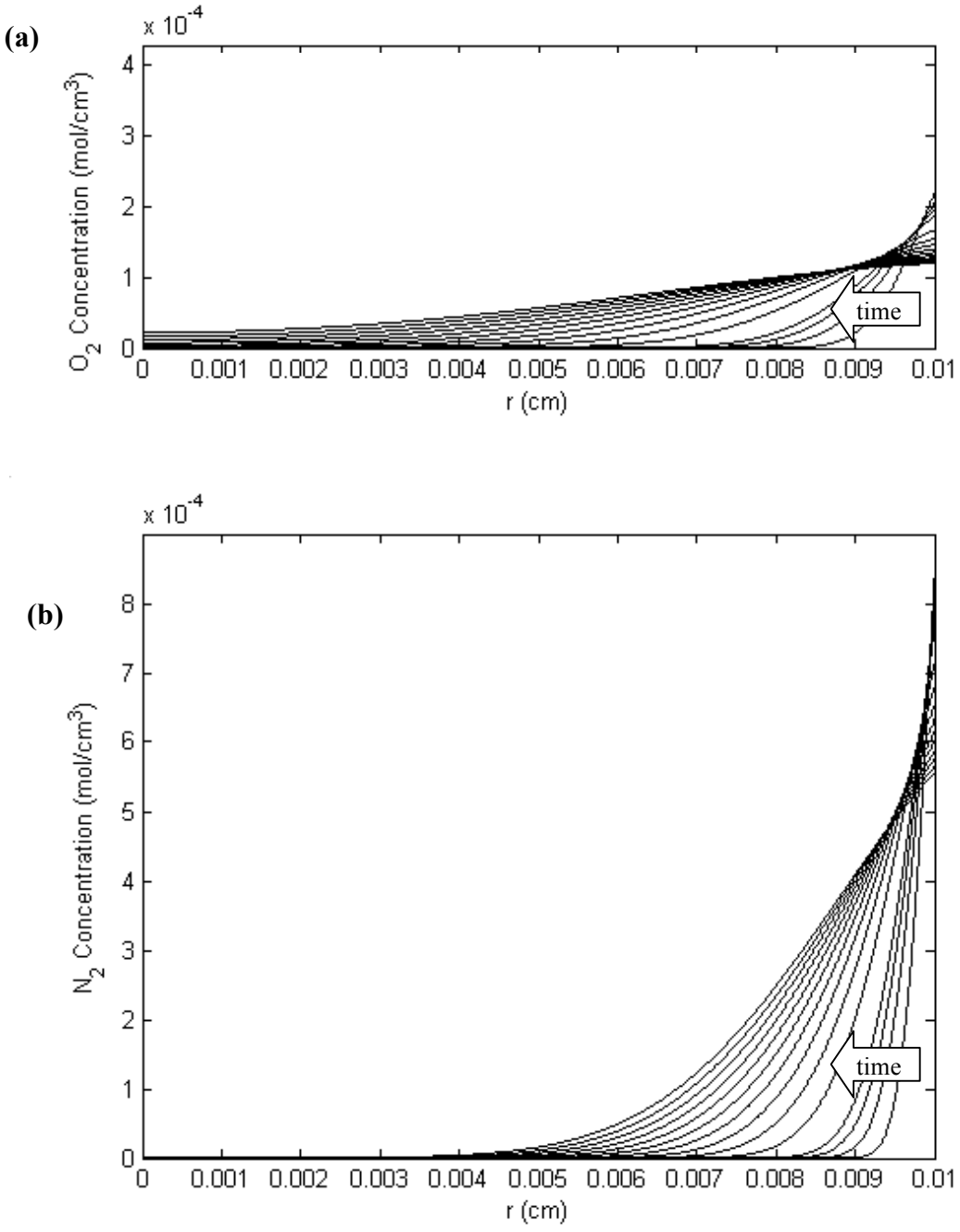

Figure 4.11. Plots of the concentration profiles for the *initial sorption step* in the spherical polymer particles over time for pressure-swing sorption air separation (21% O_2, 79% N_2) using copolymer 6FDA-durene/mPDA. (a) O_2 sorption concentration profiles. (b) N_2 sorption concentration profiles. The time steps were t = 0.5 1 1.5 2 4 6 8 10 12 14 16 18 20 22s.

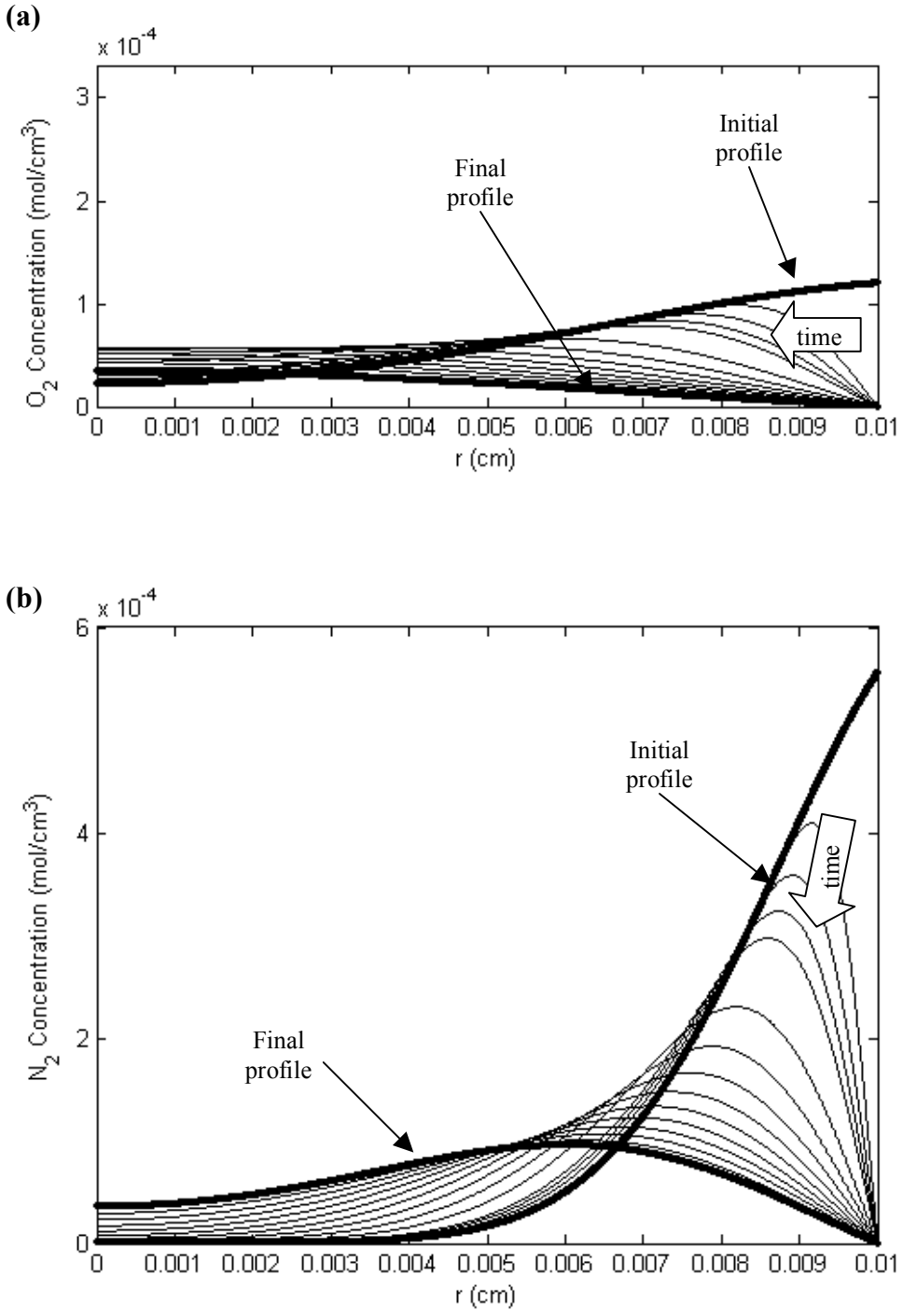

Figure 4.12. Plots of concentration profiles for the *initial desorption step* in 6FDA-durene/mPDA (80/20) copolymer particles over time for pressure-swing sorption air separation (21% O_2, 79% N_2). (a) O_2 desorption concentration profiles. (b) N_2 desorption concentration profiles. Initial and final profiles are highlighted. The time steps were t = 1 2 3 4 8 12 16 20 24 28 32 36 40 44s

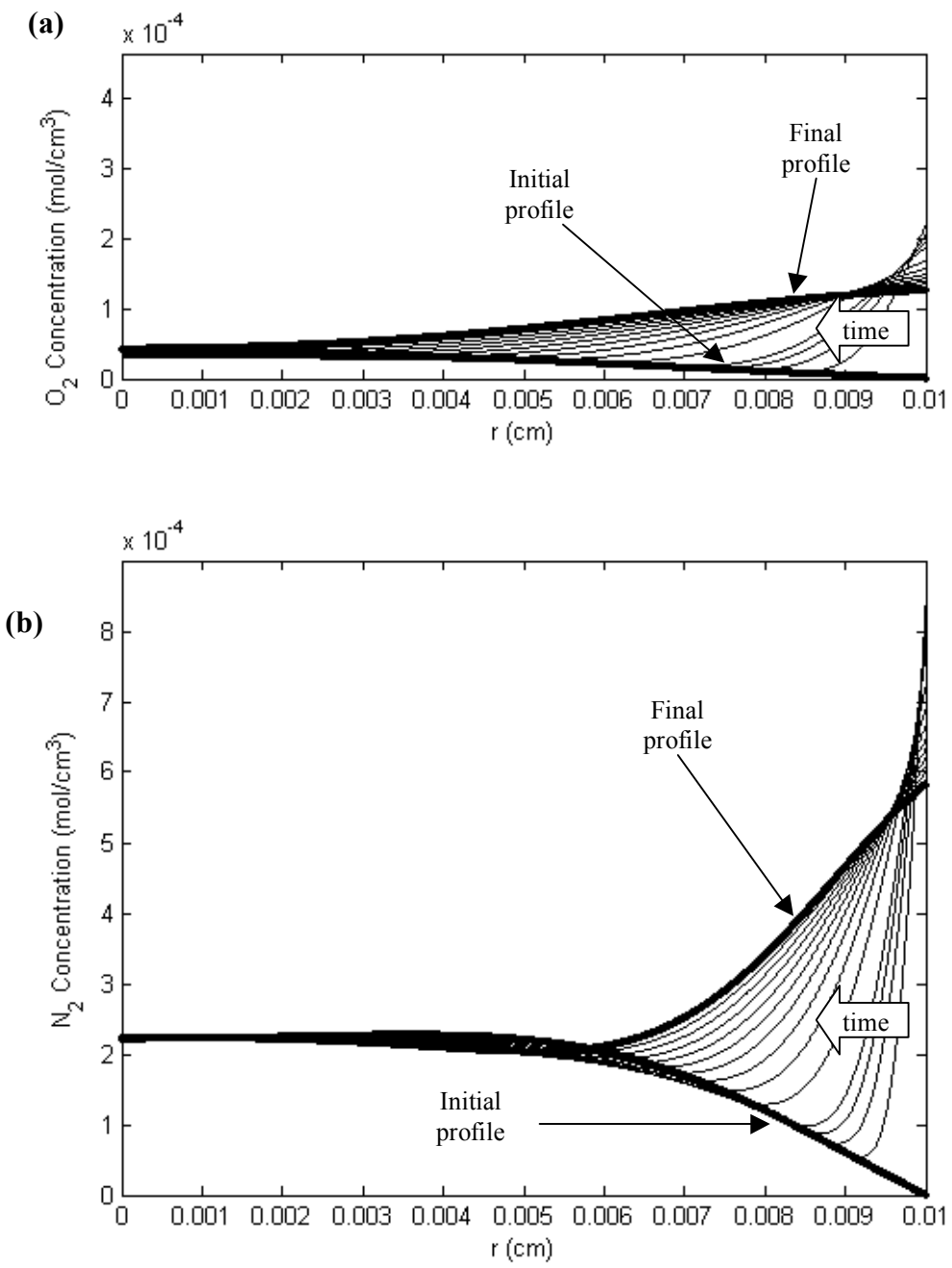

Figure 4.13. Plots of the *'steady-state' sorption* concentration profiles in the spherical polymer particles over time for pressure-swing sorption air separation (21% O_2, 79% N_2) using copolyimide 6FDA-durene/mPDA. (a) O_2 sorption concentration profiles. (b) N_2 sorption concentration profiles. The time steps were t = 0.5 1 1.5 2 4 6 8 10 12 14 16 18 20 22s.

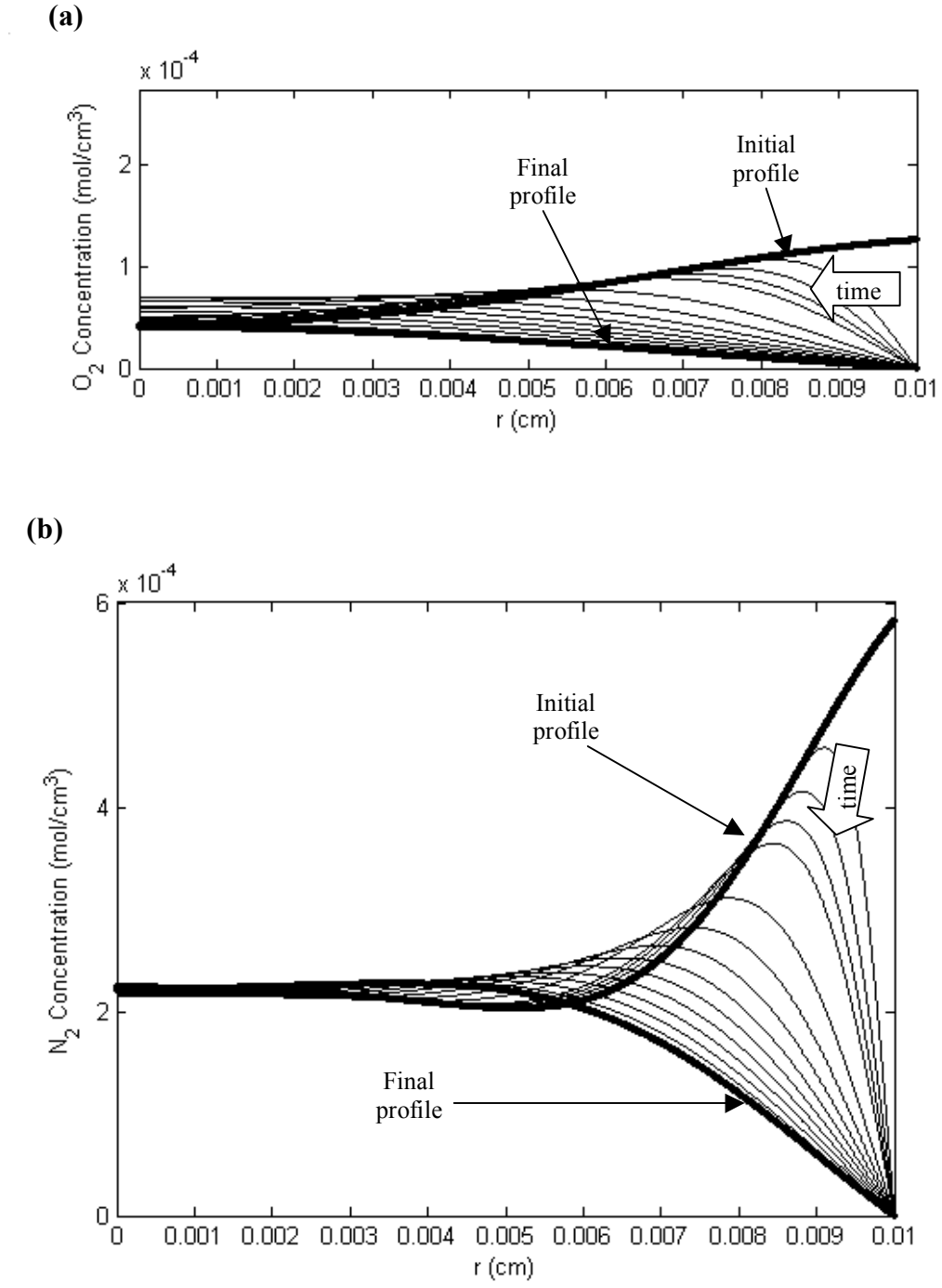

Figure 4.14. Plots of *'steady-state' desorption* concentration profiles in copolyimide 6FDA-durene/mPDA (80/20) over time for pressure-swing sorption air separation (21% O_2, 79% N_2). (a) O_2 desorption concentration profiles. (b) N_2 desorption concentration profiles. Initial and final profiles are highlighted. The time steps were t = 1 2 3 4 8 12 16 20 24 28 32 36 40 44s.

(a)

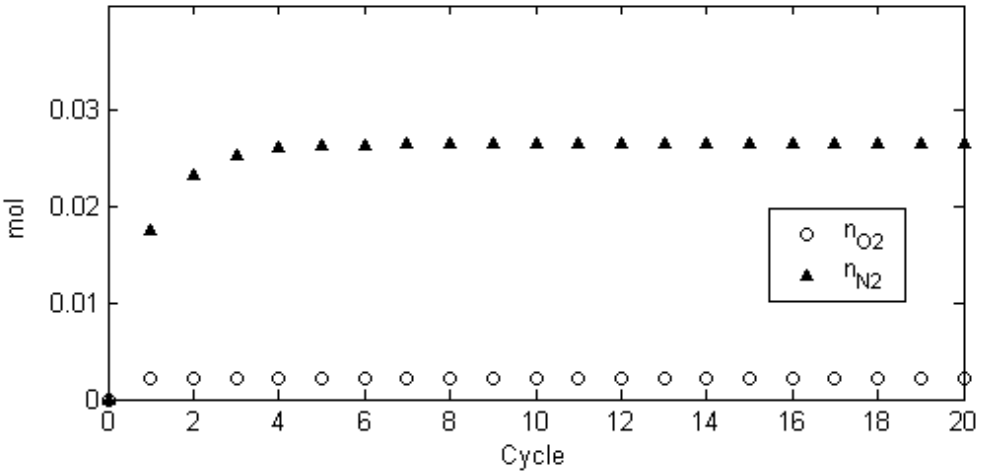

(b)

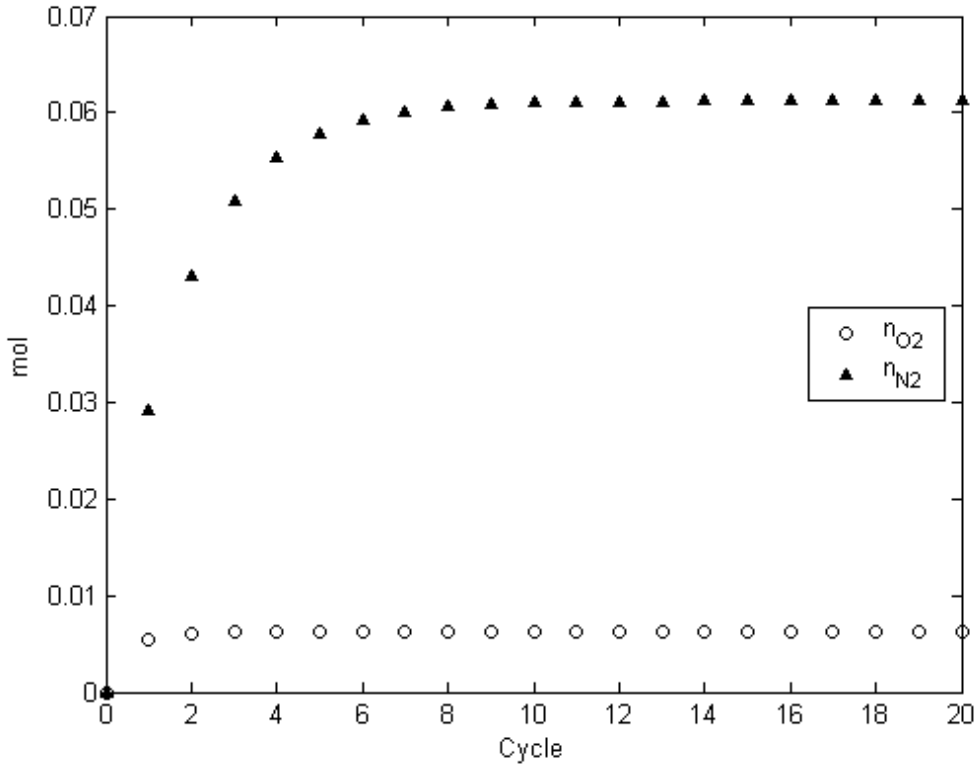

Figure 4.15. Plot of moles of O_2 and N_2 remaining in the polymer particles after successive cycles based on a 21/79 (O_2/N_2) feed mixture at 20 atm, 1L total volume, and equal volumes of polymer and external phases. (a) 6FDA-DAF. (b) 6FDA-durene/mPDA (80/20) copolyimide.

Process	Sorption Step (Gas Phase)		Desorption Step (Gas Phase)		
	X_{O2} / X_{N2}	Step Time (s)	Stage Cut (θ)	X_{O2} / X_{N2}	Step Time (s)
***Pressure-Swing Sorption*:**					
6FDA-DAF (1st Stage)	0.15 / 0.85	64	0.33	0.34 / 0.66	128
6FDA-durene/ mPDA (80/20) (1st Stage)	**0.17 / 0.83**	22	0.40	**0.28 / 0.72**	44
6FDA-durene/ mPDA (80/20) (2nd Stage w/ 1st Stage Sorption Product)	**0.13 / 0.87**	22	0.39	0.22 / 0.78	44
6FDA-durene/ mPDA (80/20) (2nd Stage w/ 1st Stage Desorption Product)	0.22 / 0.78	22	0.42	**0.35 / 0.65**	44
Membrane:					
6FDA-durene/ mPDA (80/20)	**0.12 / 0.88** (retentate)	--	0.40	**0.35 / 0.65** (permeate)	--

Table 4.4. Results for air separation (O_2 = 21%, N_2 = 79%) using the pressure-swing sorption process. 2nd stage calculations for 6FDA-durene/mPDA used the mole fractions from the sorption step and desorption purges from the 1st stage as a feed ratio and a pressure of 20 atm. These results can be compared to a membrane calculation;[16] results are listed in the last row of the table. 6FDA-durene/mPDA (80/20) copolymer characteristics were used for the membrane calculations.

4.4.2 Comparison to Membrane Technology for O_2/N_2 Separation

The same procedure in Section 4.3.2 was used to compare this process with a membrane composed of the same polymer; the active layer of the membrane was assumed to be 1000Å as before. The flow rates for feed and permeate were set using the number of moles of feed and moles removed from the polymer at the end of the desorption step, respectively, divided by the total cycle time.

These calculations show the pressure-swing separation process for O_2/N_2 is comparable to membrane separation using 6FDA-durene/mPDA (80/20). The membrane has a 4.9% higher degree of separation relative to the sorption step (equivalent to the membrane retentate) when using polymer particles. Additional separation can be achieved by adding a second stage to the pressure-swing process by further separating the purge from the sorption step, improving separation relative to the membrane (within 1%). The gas from the desorption step can also be separated further using a second separation bed, obtaining the same separation results as a membrane composed of the same polymer. These results can also be seen in Table 4.4. Similar to the CO_2/CH_4 pressure-swing separation results, the second stage desorption of the first stage sorption step (x_{A5}, x_{B5} in Figure 4.10) and the second stage sorption of the first stage desorption step (x_{A6}, x_{B6} in Figure 4.10) have compositions nearly identical to the original O_2/N_2 feed (Table 4.4). This suggests that these streams may be recycled back to the feed for greater process efficiency.

These membrane calculations assume that membranes composed of 6FDA-ODA and 6FDA-durene/mPDA can be constructed with an active layer as small as 1000Å. As a result of their stiff backbones, polyimides are very brittle and are difficult materials to use in membrane or fiber construction. Many current membrane gas separation processes use polysulfones, cellulosics, or polyamides because of their lower production costs and relative ease of manufacture.[2,4] The polymer particle process can potentially allow more ease in producing a gas separation system that can utilize the separation characteristics of polyimides.

Chapter 5: Conclusions

Based on the simulation results presented here, the pressure-swing sorption separation process has potential for application since its separation compares favorably with polymeric membrane gas separation. The transport properties of the polyimide 6FDA-ODA and copolyimide 6FDA-durene/mPDA (80/20), result in the excellent separation of the binary gas mixtures, CO_2/CH_4 and O_2/N_2, respectively. In addition, there also exists the potential to increase separation by adding multiple stages to the process.

The polymers selected for use in this process are very specific to the components of interest and are selected based on their intermolecular and physical interactions with the gases to be separated. High diffusivities, moderate diffusion ratios, high solubilities, and high solubility ratios are the polymer characteristics that provide the best separation for this process. A large difference in diffusivities can result in an excess mass retention of the more slowly diffusing species and significantly lengthen the desorption time scale needed to overcome this issue.

Since this process is untried in practice, there is much additional research that should be completed to further affirm its potential. Future models should include the issue of a distribution of polymer particle radii and its effects on the separation process. Scale-up issues such as temperature distribution and production rate should also be addressed. A more rigorous approach to optimizing the desorption time scale could potentially result in decreasing the overall cycle time for the process, allowing for greater

process efficiency. Once many of these issues have been modeled, a physical replica of this process should be developed and compared to the model results. Finally, to assess its potential commercial use, the issue of recompressing both product streams must also be addressed, as pressure-swing adsorption and membrane separation only require the re-pressurization of a single stream.

The fact that this process uses polymer particles rather than a thin membrane or hollow fiber construction, allows for more ease in manufacturing. This process also lends itself to the use of other 'super separating' polymers that have yet to be formed into membranes due to their stiff backbones and overall brittleness. Even though there are many more issues to address, pressure-swing sorption in polymer particles shows promise as an alternative method for gas separation. In addition, the potential of two-phase, core-shell particles and polymer coated porous adsorbents traditionally used in pressure-swing adsorption may further expand the possibilities of the dynamic sorption process presented in this work.

Appendix: Matlab Code for Simulation

The Matlab code listed in this appendix was written to determine the concentration profiles with increasing time over the radius of the polymer particle based on the model developed in Chapter 2. This code includes only information for the first cycle (sorption and desorption steps). The calculations for the mass in the polymer and external phases, as well as their respective compositions at given times, are included. Additional cycles can be simulated by applying the subsequent profiles in the polymer particles at the beginning of each step. The same matrices AA and BB (developed for the sorption step), and AA2 and BB2 (developed for the desorption step) can be used to calculate the sorption and desorption profiles, respectively, for components A and B for the follow-on cycles. The code below calls Matlab functions as well as M-files written by Adomaitis.[9] The M-files written by Adomaitis are described in Reference 9.

```
% Diffusion into a spherical polymer pellet, finite concentration BC
% Sorption and Desorption Cycles

addpath mcps/class
addpath mcps/class/double
close all; clear all;

                % compressibility assumed to be 1 (Z=1)
R = 5e-03;      % radius of pellet in cm
Da = 3.58e-08;  % diffusion coefficient, component A
Db = 0.220e-08; % diffusion coefficient, component B
Rg = 82.0575;   % gas constant (cm^3*atm/mol*K)
T = 308;        % temp in K
Pa = 10;        % partial pressure of component A in atm
Pb = 10;        % partial pressure of component B in atm
Ve = 500;       % external phase volume (total = 1L) (5e02 cm^3)
Vp = 500;       % volume of polymer (assuming vol frac of 0.5)
Sa = 5.52;      % partition coefficient for component A
Sb = 1.49;      % partition coefficient for component B
```

```
Np = Vp*(3/4)/(pi*(R^3));   % # of particles

xa0 = Pa/(Pa+Pb);
xb0 = Pb/(Pa+Pb);

% Quadrature/solver info/equation setup
J = 250;
nqp = 10*J;
r = quadgrid('sphe', nqp, 'r', [0,R]);
DDr = linearoperator(r, 'dd', 'r');

% Find basis functions/BC from SL problem
Psi = basisfunsl(r, 'r', 1,0,0,1);
Psi = truncate(Psi, J);
lam = eig(Psi);

% Initial conditions--polymer phase
fa0 = Sa*Pa/(Rg*T);           % conc. BC at t=0 at r=R in (mol/cm^3)
fb0 = Sb*Pb/(Rg*T);
a0 = wip(scalarfield(r,0-fa0),Psi);
b0 = wip(scalarfield(r,0-fb0),Psi);

% Setup of MX to find coefficients ai
%
% [da1/dt] = [M(1,1)  M(1,2)...M(1,J)] [a1]
% [da2/dt] = [M(2,1)  M(2,2)...M(2,J)] [a2]
% ...
% [daJ/dt] = [M(J,1)  M(J,2)...M(J,J)] [aJ]

Ka = Sa*Da*(Vp/Ve)*(3/R);
Kb = Sb*Db*(Vp/Ve)*(3/R);
I = wip(Psi);

% establish basis function derivatives
dr = linearoperator(r, 'd', 'r');
dPsi = dr*Psi;
for k = 1:J
    dPsf(k) = bf2sf(dPsi,k);
end

A = zeros(J,J);
for i = 1:J                    % rows of MX
    for j = 1:J                % columns of MX
        A(i,j) = (I(i))*Ka*(getval(dPsf(j),nqp));
    end
end

B = zeros(J,J);
for i = 1:J
    for j = 1:J
        B(i,j) = (I(i))*Kb*(getval(dPsf(j),nqp));
    end
end

%add eigenvalue terms to main diagonal of MX
A = diag(lam)*Da + A;
```

```
B = diag(lam)*Db + B;

%add df/dt row & zeros column to ends (J+1) of MX
Fa = zeros(1,J);
for n = 1:J
    Fa(n) = -Ka*(getval(dPsf(n),nqp));
end

Fb = zeros(1,J);
for n = 1:J
    Fb(n)= -Kb*(getval(dPsf(n),nqp));
end

AA = [A;Fa];
AA = [AA zeros(J+1,1)];
BB = [B;Fb];
BB = [BB zeros(J+1,1)];

%Solve ODEs in MX-vector form for a given time interval and step
tinit = 0;
tstep1 = 0.1;
tstep2 = 1;
tfinal = 86;
t = [tstep1:tstep1:tstep2, tstep2:tstep2:tfinal];   %time interval (s)

CaMx = lodesolver(AA,t, [a0;fa0],0);   %solve system of ODEs in AA Mx
CbMx = lodesolver(BB,t, [b0;fb0],0);   %solve system of ODEs in BB Mx

%PLOT OF SORPTION CONCENTRATION PROFILES--CYCLE 1
ainitmol = (Pa/(Rg*T))*Ve;            %(initial # of moles)
binitmol = (Pb/(Rg*T))*Ve;

figure(1); clf;
hold on
for k = 1:length(t)
    fa(k) = CaMx(end, k);
    fb(k) = CbMx(end, k);
    Ca = fa(k) + CaMx(1:end-1, k)*Psi;
    Cb = fb(k) + CbMx(1:end-1, k)*Psi;
    plot(Ca, 'b')
    plot(Cb, 'r')
    ma = Np*(wip(Ca));
    mb = Np*(wip(Cb));
    maex = ainitmol - ma;
    mbex = binitmol - mb;
end

title('Sorption Concentration Profiles for CO_2 and CH_4')
xlabel('r (cm)')
ylabel('Concentration (mol/cm^3)')
legend('CO_2','CH_4',0)

% DESORPTION CONCENTRATION PROFILES--CYCLE 1
mapolybeforedesorb(1) = ma;             % mol (polymer phase)
mbpolybeforedesorb(1) = mb;
xapolybeforedesorb(1) = ma/(ma+mb);     % mole frac (polymer phase)
xbpolybeforedesorb(1) = mb/(ma+mb);
```

```
maexbeforedesorb(1) = ainitmol - ma;    % ext. phase (before desorb)
mbexbeforedesorb(1) = binitmol - mb;
xaexbeforedesorb(1) = maex/(maex+mbex); % mole frac (before desorb)
xbexbeforedesorb(1) = mbex/(maex+mbex);

P2 = 0;     % desorb pressure in atm
aexintermedmol = xaexbeforedesorb*P2/(Rg*T)*Ve;  % ext. comp w/ new P
bexintermedmol = xbexbeforedesorb*P2/(Rg*T)*Ve;

fa1 = Sa*xaexbeforedesorb*P2/(Rg*T); % IC for desorption
fb1 = Sb*xbexbeforedesorb*P2/(Rg*T);
Ca1 = fa(k) + CaMx(1:end-1, k)*Psi;  % final sorption profile (new IC)
Cb1 = fb(k) + CbMx(1:end-1, k)*Psi;
a2 = wip(Ca1-fa1,Psi);               % new ai for new IC
b2 = wip(Cb1-fb1,Psi);

figure(2); clf;
hold on
plot(Ca1, 'g.')
plot(Cb1, 'm.')

Ve2 = 5e30;   % reset external phase volume to model infinite reservoir
Ka2 = Sa*Da*(Vp/Ve2)*(3/R);
Kb2 = Sb*Db*(Vp/Ve2)*(3/R);

A2 = zeros(J,J);
for x = 1:J                    % rows of MX
    for y = 1:J                % columns of MX
        A2(x,y) = (I(x))*Ka2*(getval(dPsf(y),nqp));
    end
end

B2 = zeros(J,J);
for x = 1:J
    for y = 1:J
        B2(x,y) = (I(x))*Kb2*(getval(dPsf(y),nqp));
    end
end

%add eigenvalue terms to main diagonal of MX
A2 = diag(lam)*Da + A2;
B2 = diag(lam)*Db + B2;

%add df/dt row & zeros column to ends (J+1) of MX
Fa2 = zeros(1,J);
for m = 1:J
    Fa2(m) = -Ka2*(getval(dPsf(m),nqp));
end

Fb2 = zeros(1,J);
for m = 1:J
    Fb2(m) = -Kb2*(getval(dPsf(m),nqp));
end

AA2 = [A2;Fa2];
AA2 = [AA2 zeros(J+1,1)];
BB2 = [B2;Fb2];
```

```
BB2 = [BB2 zeros(J+1,1)];

% time interval for desorption
tinit2 = 0;
tstep21 = 3*tstep1;
tstep22 = 3*tstep2;
tfinal2 = 3*tfinal;
t2 = [tstep21:tstep21:tstep22, tstep22:tstep22:tfinal2];

CaMx2 = lodesolver(AA2,t2, [a2;fa1],0);
CbMx2 = lodesolver(BB2,t2, [b2;fb1],0);

for m = 1:length(t2);
    fa2(m) = CaMx2(end, m);
    fb2(m) = CbMx2(end, m);
    Ca2 = fa2(m) + CaMx2(1:end-1,m)*Psi;
    Cb2 = fb2(m) + CbMx2(1:end-1,m)*Psi;
    plot(Ca2, 'b');
    plot(Cb2, 'r');
    ma2 = Np*(wip(Ca2));
    mb2 = Np*(wip(Cb2));
end

plot(Ca2, 'c.')
plot(Cb2, 'y.')
ylabel('Concentration (mol/cm^3)')
xlabel('r (cm)')
legend('initial profile CO_2','initial profile CH_4','CO_2','CH_4',0)
title('Desorption Concentration Profiles for CO_2 and CH_4')
hold off

apolyfinalmoles(1) = ma2;           % mass in polymer phase
bpolyfinalmoles(1) = mb2;
xapolyfinal(1) = ma2/(ma2+mb2);     % comp. in polymer phase
xbpolyfinal(1) = mb2/(ma2+mb2);
aexmolesremoved(1) = ma + aexintermedmol - ma2;   % moles extracted
bexmolesremoved(1) = mb + bexintermedmol - mb2;
xamolesremoved(1) =
aexmolesremoved(1)/(aexmolesremoved(1)+bexmolesremoved(1)); % comp.
xbmolesremoved(1) =
bexmolesremoved(1)/(aexmolesremoved(1)+bexmolesremoved(1));
```

Bibliography

1. R. Prasad, R.L. Shaner, and K.J. Doshi in Polymeric Separation Membranes, edited by D.R. Paul, Yuri P. Yampol'skii, (CRC Press, Boca Raton, 1994), pp 598-599.

2. J.M.S. Henis in Polymeric Separation Membranes, edited by D.R. Paul, Yuri P. Yampol'skii, (CRC Press, Boca Raton, 1994), pp 451, 478, 483, 485, 490.

3. H. Ohya, V.V. Kudryavtsev, S.I. Semenova, Polyimide Membranes: Applications, Fabrications, and Properties, (Gordon and Breach, Amsterdam, 1996), pp 1, 103-104, 110, 112, 123, 260-261.

4. H. Kawakami, J. Anzai and S. Nagaoka, "Gas transport properties of soluble aromatic polyimides with sulfone diamene moieties," J. Appl. Polym. Sci., 57, 789 (1995).

5. H. Kawakami, K. Nakajima, and S. Nagaoka, "Gas separation characteristics of isomeric polyimide membrane prepared under shear stress," J. Membr. Sci., 211, 291, (2003).

6. J-J. Qin, T-S. Chung, C. Cao, and R.H. Vora, "Effect of temperature of intrinsic permeation properties of 6FDA-durene/1,3 phenylenediamene (mPDA) copolyimide and fabrication of its hollow fiber membranes for CO_2/CH_4 separation," J. Membr. Sci., 250, 95 (2005).

7. H. Kawakami, K. Nagajima, H. Shimizu, and S. Nagaoka, "Gas permeation stability of asymmetric polyimide membrane with thin skin layer: effect of polyimide structure," J. Membr. Sci. 212, 195, (2003).

8. T.A. Barbari, S.S. Kasargod, and G.T. Fieldson, "Effect of unequal transport rates and intersolute salvation on the selective batch extraction of a dilute mixture with a dense polymeric solvent," Ind. Eng. Chem. Res. 35, 1188 (1996).

9. R.A. Adomaitis, "Objects for MWR," Computers & Chem. Eng., 26, 981 (2002).

10. J. Crank, The Mathematics of Diffusion, 2nd ed. (Oxford University Press, New York, 1975), pp 93-94.

11. M.R. Pixton and D.R. Paul in Polymeric Separation Membranes, edited by D.R. Paul, Yuri P. Yampol'skii, (CRC Press, Boca Raton, 1994), pp 102, 105, 109, 116-119, 124, 126, 128-129.

12. T.H. Kim, "Gas Sorption and Permeation in a Series of Aromatic Polyimides," Ph. D. Dissertation, University of Texas at Austin, 1988.

13. T-S. Chung, W-H. Lin, R.H. Vora, "Gas transport properties of 6FDA-durene/1,3 phenylenediamene (mPDA) copolyimides," J. Appl. Polym. Sci., 81, 3552 (2001).

14. W.S.W. Ho and K.K. Sirkar in Membrane Handbook, edited by W.S.W. Ho and K.K. Sirkar, (Van Nostrand Reinhold, New York, 1992), p 28.

15. J.D. Wind, et al. "Relaxation dynamics of CO_2 diffusion, sorption and polymer swelling for plasticized polyimide membranes," Macormolecules, 36 6442 (2003).

16. J.D. Seader and E.J. Henley, Separation Process Principles, (John Wiley and Sons, Hoboken, 1988), pp735-738.

17. R.R. Zolandz and G.K. Fleming in Membrane Handbook, edited by W.S.W. Ho and K.K. Sirkar, (Van Nostrand Reinhold, New York, 1992), p 56.